Supplementary Information

Synthesis of Poly(Arylene Iminophosphorane)s and Various Materials Therefrom: Unlocking the Potential of Azide-Phosphine Staudinger Reaction

Tomaž Kotnik[a,b], Antoine Debuigne[c], Julien De Winter[d], Matej Huš[a,e,f], Albin Pintar[a], Sebastijan Kovačič[a,g*]

[a] T. Kotnik, A. Pintar, M. Huš, S. Kovačič

National Institute of Chemistry, Hajdrihova 19, SI-1001 Ljubljana, Slovenia

[b] T. Kotnik

Faculty of Chemistry and Chemical Technology, University of Ljubljana,

Večna pot 113, SI-1000 Ljubljana, Slovenia

[c] A. Debuigne

Center for Education and Research on Macromolecules (CERM), CESAM Research Unit, Chemistry Department, University of Liege (ULiege), Quartier Agora, 13 Allée du Six Août (Bldg B6a), Sart-Tilman, B-4000 Liège, Belgium

[d] J. De Winter

Organic Synthesis and Mass Spectrometry Laboratory (S2MOs), University of Mons-UMONS, Mons 7000, Belgium

[e] M. Huš

Association for Technical Culture of Slovenia (ZOTKS), Zaloška 65, SI-1000 Ljubljana, Slovenia

[f] M. Huš

Institute for the Protection of Cultural Heritage of Slovenia (ZVKDS), Poljanska 40, SI-1000 Ljubljana, Slovenia

[g] S. Kovačič

Catalysis and Organic Synthesis research group, Faculty of Chemistry and Chemical Engineering, University of Maribor, Smetanova 17, SI-2000 Maribor, Slovenia

E-mail: sebastijan.kovacic@um.si

Abstract: Iminophosphoranes with the general formula ($R_3P{=}NR'$) have great potential in synthetic chemistry as valuable precursors/intermediates in organic synthesis or as building blocks for various organic compounds. However, the synthetic approaches and conditions to prepare iminophosphoranes are still poorly understood, limiting the utility of this chemistry for organic materials. In this article, a simple and efficient synthesis of previously unattainable poly(aryleneiminophosphoranes) is reported. The azide-phosphine Staudinger polycondensation is used, and the reaction conditions are carefully studied, including consideration of light and air, the influence of solvent and temperature, and investigation of the electronic and steric effects of multiazides. The newly defined reaction conditions appear to be highly versatile, allowing the use of both electron-rich and electron-deficient arylazides for reaction with phosphines to synthesize a library of poly(arylene iminophosphorane) networks that exhibit exceptional thermal and oxidative stability. Interestingly, despite the ylidic-form of the iminophosphorane linkage as shown by theoretical calculations, these newly developed poly(arylene-iminophosphorane) networks exhibit semiconducting properties, such as absorption band edges up to 800 nm and optical band gaps in the range of 1.70 to 2.40 eV. Finally, we demonstrate the broad applicability of these polymers by processing them into glassy films, creating foam-like structures and synthesizing metallo-polymer hybrids.

Table of Contents

Supplementary Methods

Experimental Procedures

Characterization

NMR spectroscopy analyses were performed on Bruker Avanze NEO 400 and 600 MHz spectrometers. ^{1}H NMR spectra were carried out at room temperature in the pulse Fourier-transform mode using various deuterated solvents such as $CDCl_3$ and DMSO-d6 all purchased from Cambridge Isotope Laboratories. The relaxation delay was set to 5 s in order to guarantee complete proton relaxation. Chemical shifts are given in ppm relative to a $SiMe_4$ standard in the case of ^{1}H and ^{13}C and H_3PO_4 in the case of ^{31}P. In the case of ^{13}C and ^{31}P CP/MAS NMR spectroscopy, the 4 mm CP-MAS probe with 1H-19F and 31P-15N coils and a maximum spinning rate of 18 kHz with a delay time of 2–10 s was used. The ^{31}P NMR spectra were deconvoluted in ssNake NMR processing and fitting software. NMR data were also processed using MestReNova software.

FTIR spectroscopy was performed on the dried grinded samples using a Perkin-Elmer (Inc., Waltham, MA, USA) FTIR spectrometer with attenuated total reflection (ATR) in a 500-3500 cm^{-1} range at a resolution of 4 cm^{-1}. The presented spectra are an average of 32 consecutive measurements on Ge-crystal.

Elemental analysis was determined with a Perkin Elmer 2400 Series II CHNS/O Elemental Analyzer. Cystine was used as a calibration standard. The combustion temperature was 975 °C.

TGA analysis was used to evaluate the thermal properties of each polymer. Thermal gravimetric analysis (TGA) and differential scanning calorimetry (**DSC**) were performed using the Mettler Toledo TGA/DSC1 Star system. Thermal decomposition and oxidative stability were performed under inert (N_2) and air atmosphere, in dynamic and isothermal modes.

Scanning electron microscopy (SEM) images were collected on a Supra 35 VP scanning electron microscope from Carl Zeiss. The samples were attached to a carbon tab for better conductivity and afterward, a thin layer of Pt was sputtered on a sample's surface prior to scanning analysis (for SEM investigations). SEM micrographs were taken at various magnifications at 7 mm working distance, and 5 kV voltage was applied using secondary electron (SE) and in-lens detectors.

Nitrogen physisorption analysis was determined from the adsorption and desorption isotherms of N_2 at -196 °C using a Micromeritics TriStar II 3020 instrument. Prior to characterization, the samples were degassed under N_2 stream (purity 6.0) using a programmed bilevel heating, with the first heating stage at 90 °C for 60 min, followed by the second heating stage at 160 °C for 240 min. The heating rate was set to 10 °C min^{-1} for both heating stages. The specific surface area of the samples was calculated by applying the BET theory to the nitrogen adsorption data within the 0.06−0.30 P/P_0 range.

The polyHIPE skeletal densities (ρ_P) (an average of 10 consecutive measurements) were evaluated using a fully automated, highly precision **helium pycnometry** (Micromeritics, model AccuPyc II 1340). To prevent the influence of moisture and impurities on the measurements, the polyHIPEs were thoroughly dried and purged with nitrogen.

UV-Vis DR spectroscopy was performed on a Perkin Elmer Lambda 650 UV-Vis spectrophotometer equipped with the accessory for powdered samples (Harrick Scientific Products, Pleasantville, NY, USA) in order to record the UV-Vis diffuse reflectance spectra of the prepared materials. The background correction was performed with a white reflectance standard Spectralon® (range of 200 − 900 nm).

The size exclusion chromatography (SEC) analyses were carried out in THF at 40 °C with a flow rate of 1 mL.min-1 using a Viscotek 305 TDA chromatograph equipped with two columns (PSS SDV linear M 5 µm) and a triple detector (refractive index, viscometer, low angle light scattering) calibrated with a Malvern PS standard of 99 kDa. Data were treated with the Omnisec 4.7 software.

Matrix-assisted laser desorption/ionization time-of-flight (MALDI-ToF) mass spectra are recorded using a Waters QToF Premier mass spectrometer. A Nd-YAG laser of 355 nm with a maximum pulse energy of 65 µJ delivered to the sample at 50 Hz repeating rate is used. Time-of-flight mass analyses are performed in the reflection mode at a resolution of about 10,000. Trans-2-(3-(4-tert-butyl-phenyl)-2-methyl-2-propenylidene)malononitrile (DCTB) is used as the matrix and is prepared as a 40 mg/ml solution in chloroform. The matrix solution (1 µl) is applied to a stainless steel target and air-dried. Polymer samples are dissolved in chloroform to obtain 1 mg/mL solutions. 1 µl aliquots of these solutions are applied onto the target area (already bearing the matrix crystals) and air-dried.

Powder X-ray diffraction data (PXRD) were obtained in the 2θ range from 5 to 70° using CuKα1 radiation (1.5406 Å) on a PANanalytical X'Pert PRO high-resolution diffractometer.

Materials

The following chemicals were used: 1,4-bis(diphenylphosphino)benzene (98%), 1,1'-bis(diphenylphosphino)ferrocene (97%), 1,3,5-phenyltriboronic acid tris(pinacol) ester (97%), 1,4-benzenediboronic acid bis(pinacol) ester (98%), 2,1,3-benzothiadiazole-4,7-bis(boronic acid pinacol ester) (>98%), 9,9-dioctyl-9H-fluorene-2,7-diboronic acid bis(pinacol) ester (97%), 1,3,5-tri(4-pinacolatoborolanephenyl)benzene (98%), n-hexane (≥99%), DMF (≥99.8%), chloroform (≥99.8%), toluene (≥99.5%), methanol (≥99.8%), sodium azide (99.5%), copper(II) acetate (98%), acetone (99.8%), acetonitrile (99.8%), THF (≥99.9%), DABCO (≥99%), HQ (≥99%,), and copper(I) iodide (≥99.5%). Chemicals were used as received, except toluene and DMF, the solvents used in polymerization, which were dried using molecular sieves, and phosphine monomers, which were further refined to higher than 99% purity.

I. Synthesis of organic multiazides by Chan-Lam coupling reaction

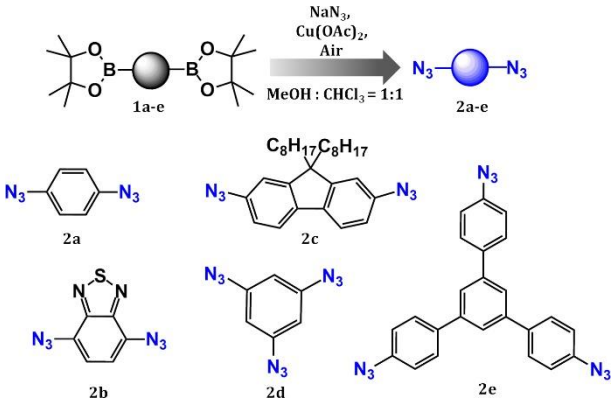

Figure S1. General conditions and scope of multiazide synthesis.

Prior to investigating the azide-phosphine Staudinger condensation reaction for the polymerization, we used the Chan-Lam coupling reaction and synthesized variously substituted organic multiazides (**Figure S1**). By combining and optimizing several already known Chan-Lam reaction protocols,[59,60] we prepared a series of multiazide precursor monomers (**2a-e**) on a gram scale, which subsequently allowed us to study their reactivity with various bis(diphenylphosphino) derivatives (**3a-b**). Cross-coupling between arylboronic acid pinacol ester derivatives and sodium azide in the presence of a Cu-catalyst leads to substituted multiazides in good to excellent yields, namely 1,4-diazidobenzene (**2a**; 98%), 4,7-diazido-1,2,5-benzothiadiazole (**2b**; 93%), 9,9-dioctyl-2,7-diazidofluorene (**2c**; 73%), 1,3,5-triazidobenzene (**2d**; 75%), and 1,3,5-tris(4-azidophenyl)benzene (**2e**; 83%). ^{1}H and ^{13}C NMR spectroscopy confirmed the formation of the desired multiazide monomers. The spectra clearly show the disappearance of the methyl proton peaks at 1.35 ppm in ^{1}H NMR, as well as the methyl carbon peaks at 25 ppm and the tertiary carbon peaks at 83 ppm in ^{13}C NMR, which are typical of the pinacol boronate ester group. FTIR spectra showed a new signal for the azide band at ~2110 cm^{-1} in all cases. The elemental analysis also confirmed the complete transformation of the pinacolboronate esters into azide groups, since the found values for the N-content were in accordance with the calculated ones. It should be noted that handling low molecular weight organic azides requires special precautions, as they can react violently when heated externally (> 150 °C or under shock).[61] Although the number of nitrogen atoms is greater than the number of carbon atoms in azides **2b** and **2d**, [62] we did not encounter any handling problems, but caution is still advised. In addition, this approach involves the use of chloroform and sodium azide, which raises concerns about the formation of unstable triazidomethane.[63] However, ^{1}H and ^{13}C NMR spectroscopy showed that these species are not present in our case.

All the characterization data is provided below.

1,4-diazidobenzene

2a

To a solution of **1a** (1.0 g, 3.0 mmol) in a mixture of methanol and chloroform (1:1), sodium azide (591 mg, 9.1 mmol) and copper (II) acetate (100 mg, 0.55 mmol) was added. The solution was aerated with compressed air at a 150 ml/min flow rate and heated (55 °C) under reflux for 16 hours. After reaction completion, the solvents were evaporated under reduced pressure, and the product was separated with dry load chromatography using hexane as an eluent.

Yield: 98 % (470 mg)

^{1}H NMR

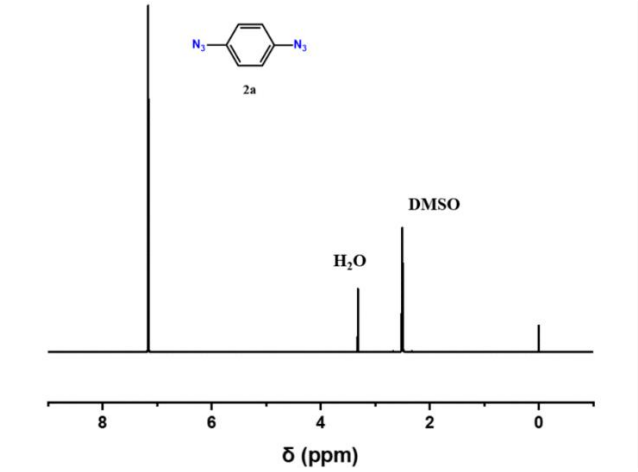

^{1}H NMR (600 MHz; DMSO-d6) δ 7.16 (4H, s).

^{13}C NMR

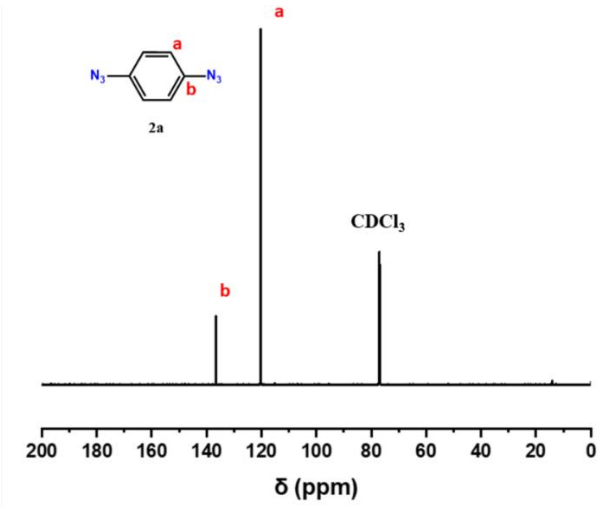

^{13}C NMR (600 MHz; $CDCl_3$): δ 136.70, 120.36.

FTIR

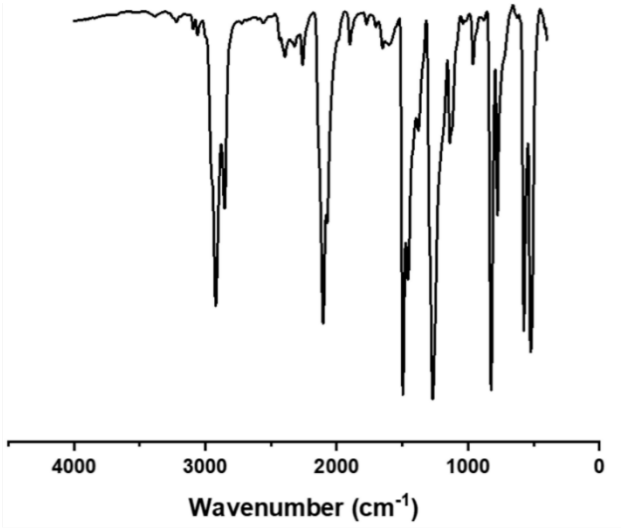

FT-IR (ATR): ν_{max} 2925, 2849, 2101 (R-N_3), 2069 (R-N_3), 1497, 1461, 1374, 1267, 1132, 957, 827, 773, 571, 516 cm^{-1}.

Elemental analysis

Element	Experimental (%)	Calculated (%)
C	46.5	45.5
H	2.8	2.5
N	49.5	52.0
S	/	/

4,7-diazido-1,2,5-benzothiadiazole

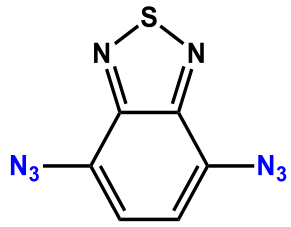

2b

To a solution of **1b** (1.164 g, 3.0 mmol) in a mixture of methanol and chloroform (1:1), sodium azide (585 mg, 9.0 mmol) and copper (II) acetate (135 mg, 0.74 mmol) was added. The solution was aerated with compressed air at a flow rate of 150 ml/min for 12 hours at an elevated temperature (55 °C). After reaction completion, the solvents were evaporated under reduced pressure, and the product was separated with dry load chromatography using acetone as eluent. To the eluate, water was added to precipitate the final product. After filtration of the product, the residual eluate was concentrated under reduced pressure to remove some of the acetone and filtrated again.

Yield: 93 % (203 mg)

^{1}H NMR

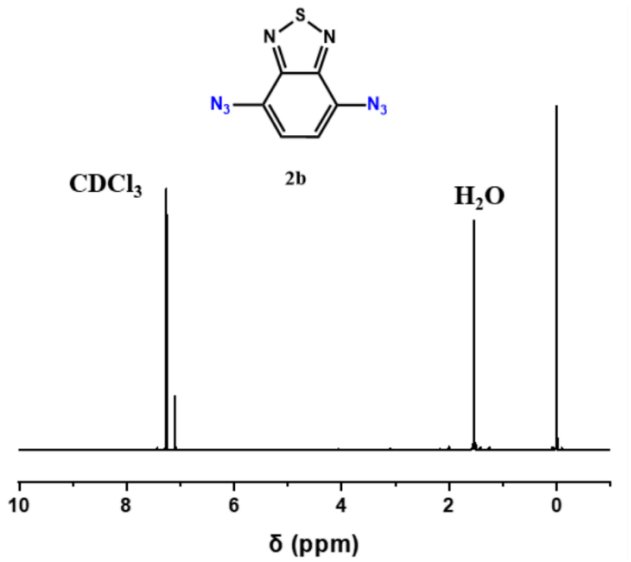

^{1}H NMR (600 MHz; $CDCl_3$) δ 7.13 (2H, s).

^{13}C NMR

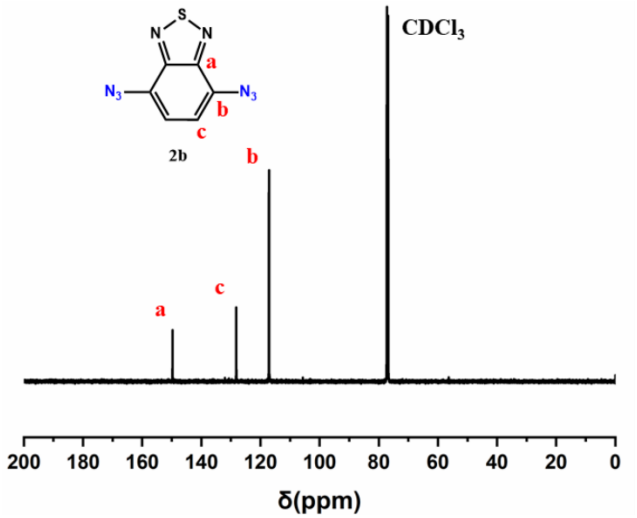

^{13}C NMR (600 MHz; $CDCl_3$) δ 149.72, 128.18, 117.12.

FTIR

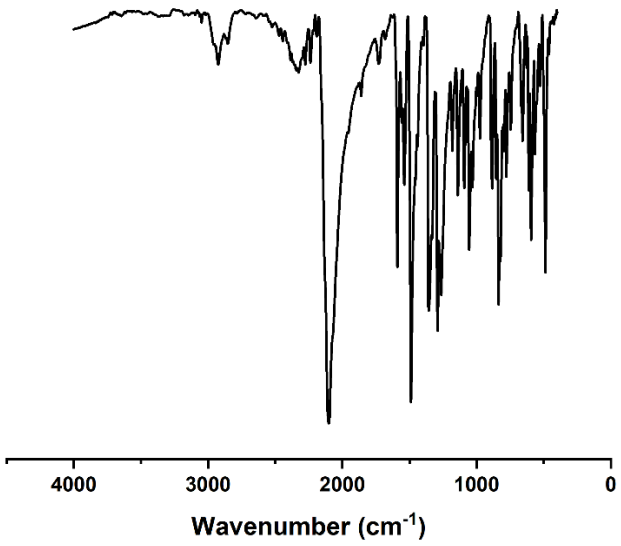

FT-IR (ATR): ν_{max} 2929, 2858, 2097 (R-N_3), 1591, 1533, 1487, 1358, 1293, 1260, 1183, 1137, 1095, 1027, 972, 886, 833, 820, 777, 744, 656, 611, 592, 564, 525, 488 cm^{-1}.

Elemental analysis

Element	Experimental (%)	Calculated (%)
C	36.0	33.3
H	1.6	1.0
N	47.0	51.0
S	14.3	14.7

9,9-Dioctyl-2,7-diazidofluorene

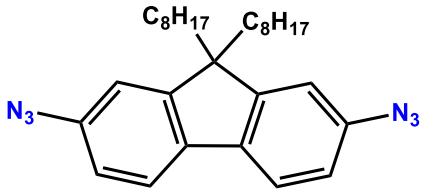

2c

To a solution of **1c** (1.084 g, 1.7 mmol) in methanol, sodium azide (280 mg, 4.3 mmol) and copper iodide (54.6 mg, 0.29 mmol) were added. The solution was aerated with compressed air at a flow rate of 150 ml/min for 18 hours at an elevated temperature (60 °C). After reaction completion, the solvents were evaporated under reduced pressure, and the product was separated with dry load chromatography using hexane as an eluent. The eluate was concentrated under reduced pressure to obtain the crude product, which was then recrystallized from acetonitrile to yield the pure product.

Yield: 73 % (584 mg)

^{1}H NMR

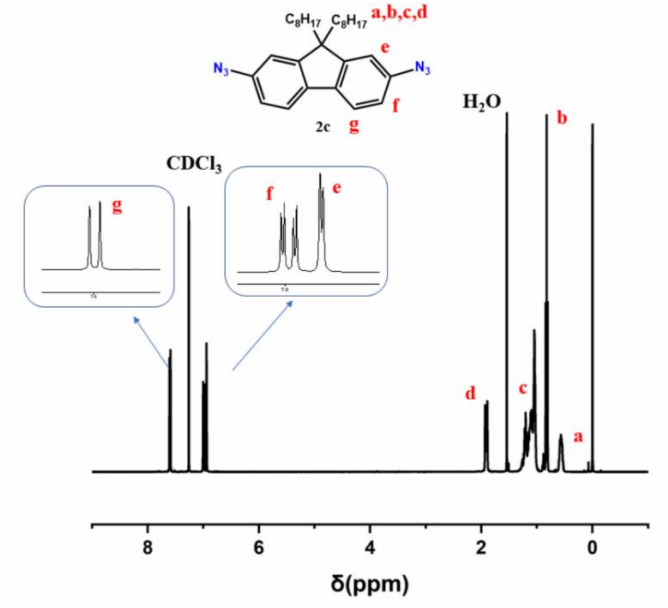

^{1}H NMR (600 MHz, $CDCl_3$) δ 7.62 (d, *J* = 8.1 Hz, 2H), 7.02 (dd, *J* = 8.1, 2.1 Hz, 2H), 6.96 (d, *J* = 2.1 Hz, 2H), 1.98 – 1.86 (m, 6H), 1.29 – 1.00 (m, 14H), 0.85 (td, *J* = 7.2, 1.7 Hz, 8H), 0.66 – 0.52 (m, 6H).

^{13}C NMR

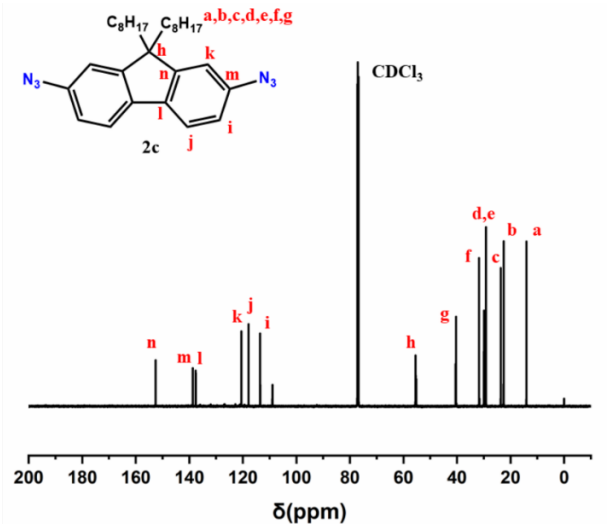

^{13}C NMR (600 MHz; $CDCl_3$) δ 152.57, 138.72, 137.60, 120.53, 117.87, 113.58, 55.45, 40.53, 40.37, 31.77, 29.95, 29.19, 23.64, 22.58, 14.05.

FTIR

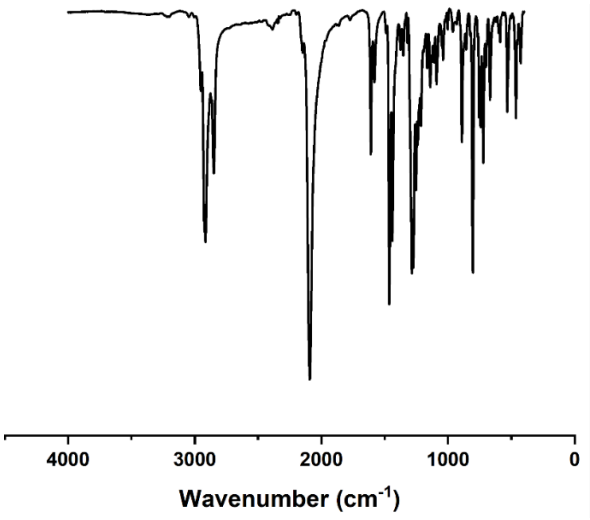

FT-IR (ATR): ν_{max} 2951, 2914, 2850, 2090 (R-N_3), 1611, 1579, 1463, 1441, 1288, 1273, 1252, 1214, 890, 805, 755, 744, 722, 670, 532, 465, 428 cm^{-1}.

Elemental analysis

Element	Experimental (%)	Calculated (%)
C	74.4	73.7
H	8.0	8.5
N	16.5	17.8
S	/	/

1,3,5-triazidobenzene

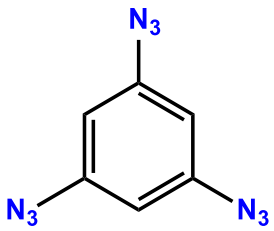

2d

To a solution of **1d** (912 mg, 2.0 mmol) in a mixture of chloroform and methanol (1:2) sodium azide (644 mg, 9.9 mmol) and Cu(II) acetate (100 mg, 0.55 mmol) was added. The reaction was heated at 55 °C under reflux for 16 h and aerated with compressed air at a 150 ml/min flow rate. After reaction completion, the residue was filtered and washed with acetonitrile. The product precipitated after the addition of water into the filtrate. The crude product was further recrystallized from hexane to yield the solid white product.

Yield: 75 % (314 mg)

^{1}H NMR

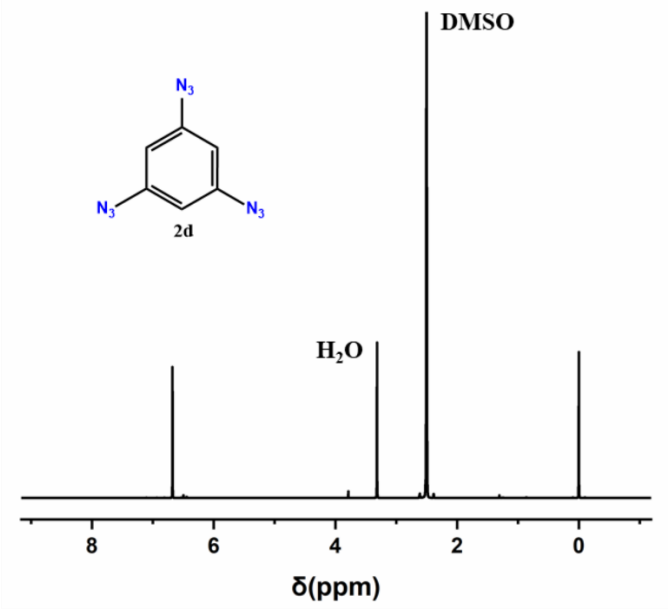

^{1}H NMR (600 MHz, DMSO-d_6): δ 6.68 (s, 3H).

^{13}C NMR

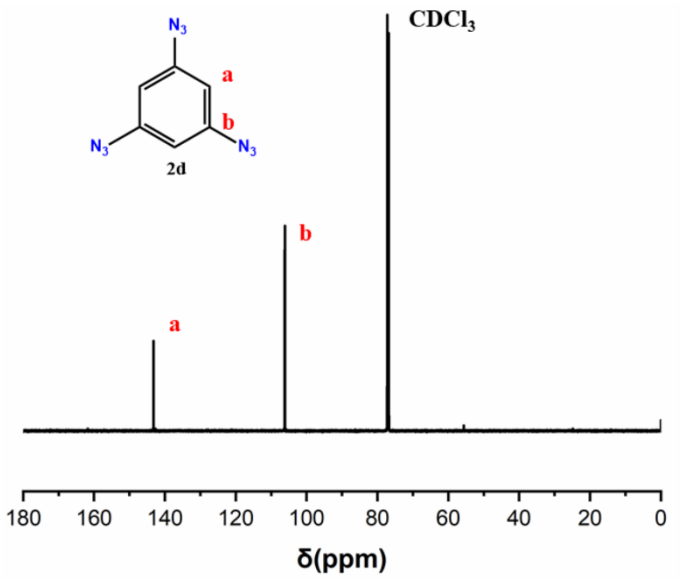

^{13}C NMR (600 MHz; $CDCl_3$): δ 143.22, 106.15.

FTIR

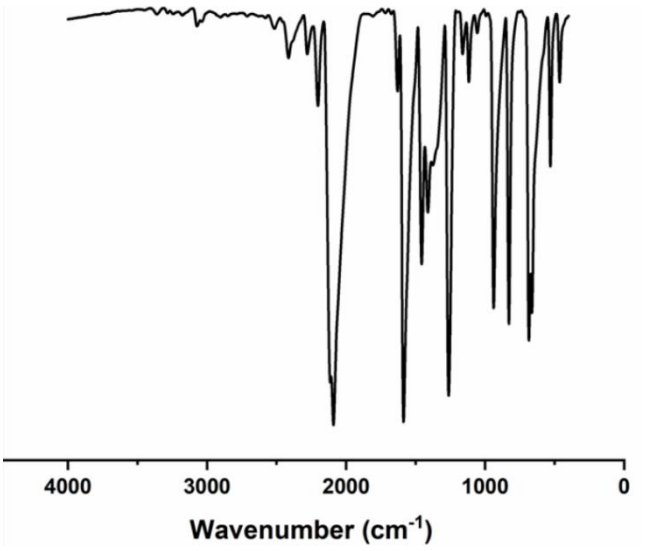

FT-IR (ATR): ν_{max} 3080, 2087 (R-N_3), 1624, 1584, 1454, 1406, 1259, 1112, 941, 831, 687, 665, 528, 462 cm^{-1}.

Elemental analysis

Element	Experimental (%)	Calculated (%)
C	36.7	35.8
H	1.9	1.5
N	59.5	62.7

1,3,5-Tris(4-azdidophenyl)benzene

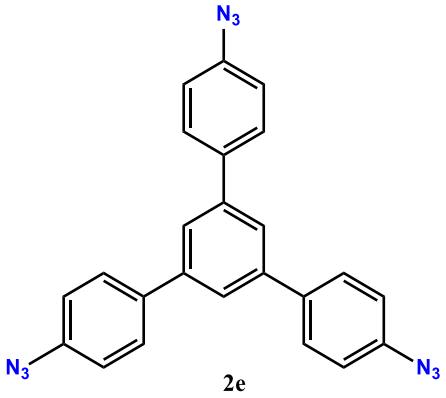

2e

To a solution of **1e** (260 mg, 0.38 mmol) in a mixture of methanol and chloroform (1:1) sodium azide (195 mg, 3.0 mmol) and copper(II) acetate (42 mg, 0.23 mmol) were added. The solution was aerated with compressed air at a flow rate of 150 ml/min for 18 hours at an elevated temperature (55 °C). Additional sodium azide (65 mg, 1 mmol) and copper(II) acetate (20 mg, 0.11 mmol) were added, and the reaction mixture was again heated for 12 h. After reaction completion, the solvents were evaporated under reduced pressure, and the residue was dissolved in hot acetonitrile. The solid residue was filtered off, and the product was precipitated by the addition of water into the cooled acetonitrile solution and filtered off.

Yield: 83 % (134 mg)

^{1}H NMR

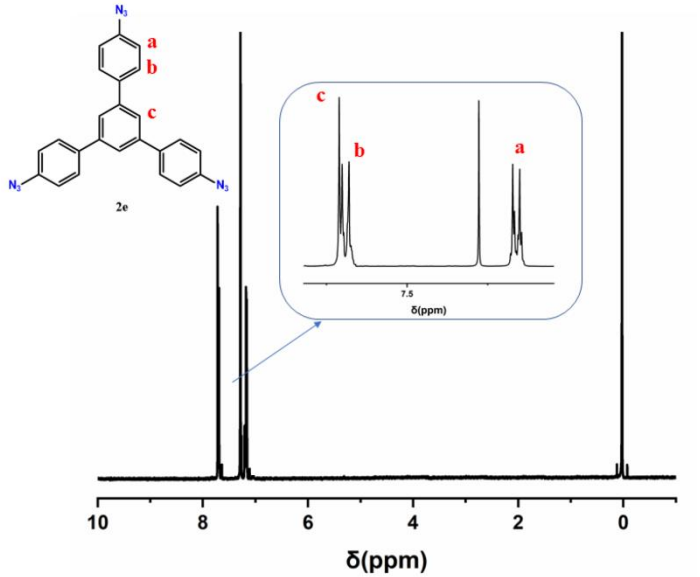

^{1}H NMR (600 MHz, $CDCl_3$): δ 7.72 (s, 3H), 7.70 (d, *J* = 8.5 Hz, 6H), 7.17 (d, *J* = 8.6 Hz, 6H).

^{13}C NMR

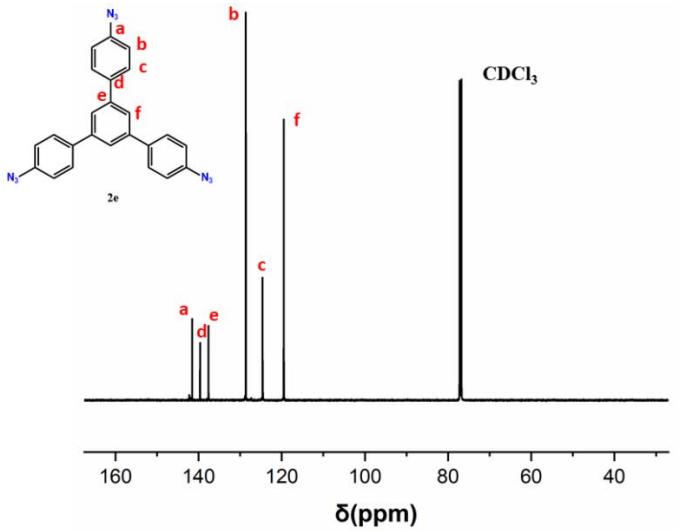

^{13}C NMR (600 MHz; $CDCl_3$): δ 141.53, 139.64, 137.61, 128.63, 124.60, 119.52.

FTIR

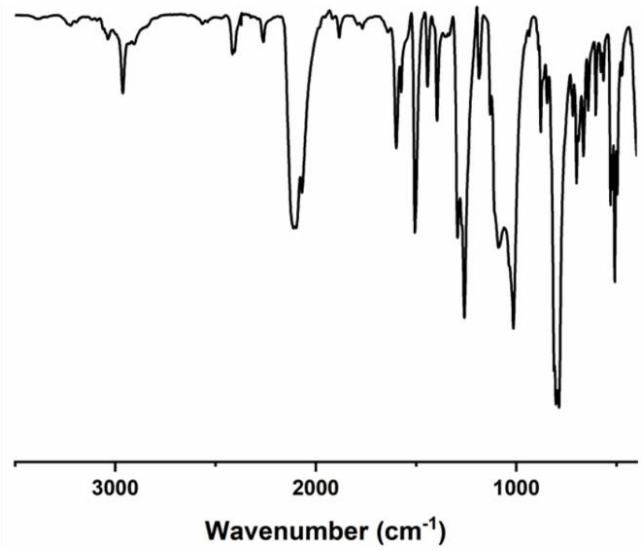

FT-IR (ATR): ν_{max} 2961, 2405, 2111 (R-N_3), 1601, 1573, 1507, 1440, 1393, 1291, 1260, 1189, 1092, 1017, 880, 804, 701, 667, 508 cm^{-1}.

Elemental analysis

Element	Experimental (%)	Calculated (%)
C	67.9	67.1
H	3.8	3.5
N	26.8	29.4
S	/	/

II. Commercial monomers characterization

1,4-Bis(diphenylphosphino)benzene

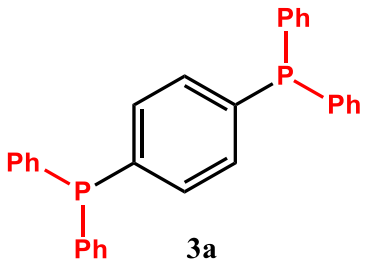

3a

^{13}C CP/MAS

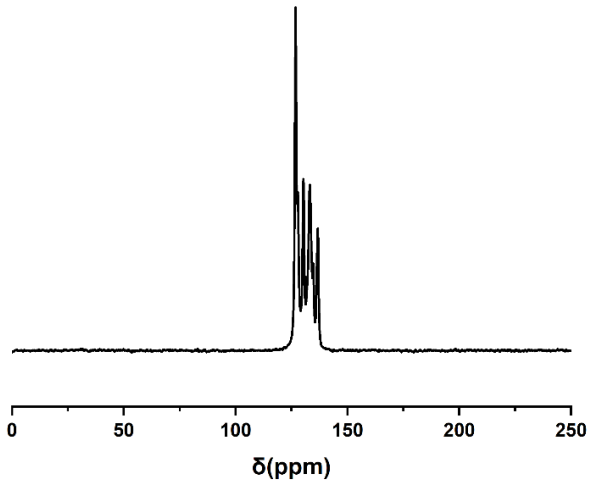

^{13}C CP/MAS NMR (400 MHz): δ 136.7, 134.7, 133.2, 130.3, 127.8, 126.8.

^{31}P CP/MAS

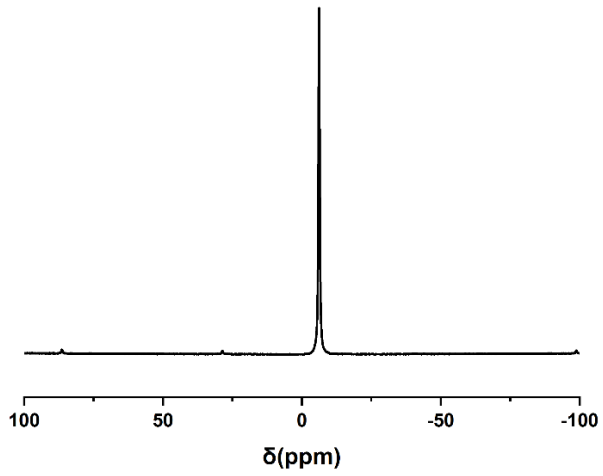

^{31}P CP/MAS NMR (400 MHz): δ - 6.19.

1,1′-Ferrocenediyl-bis(diphenylphosphine) – DPPF

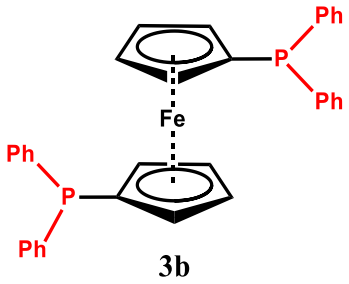

3b

^{13}C CP/MAS NMR

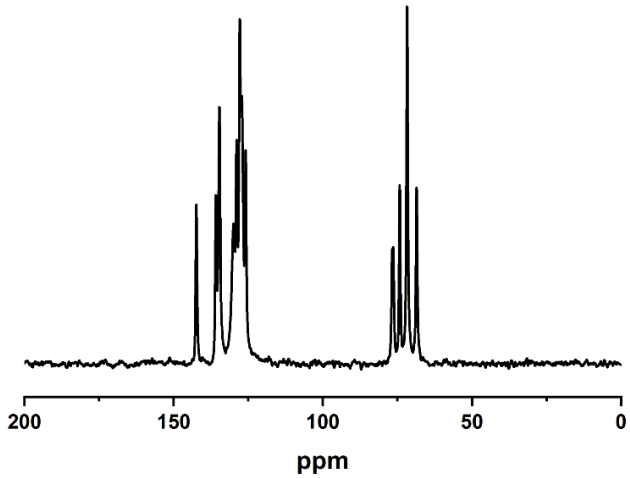

^{13}C CP/MAS NMR (400 MHz): δ 142.41, 135.84, 134.65, 129.93, 128.90, 127.82, 127.17, 125.87, 76.64, 74.24, 71.72, 68.55.

^{31}P CP/MAS

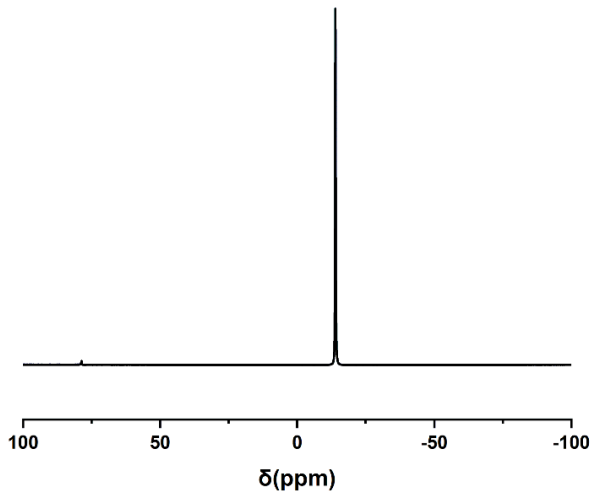

^{31}P CP/MAS NMR (400 MHz): δ - 13.94.

III. Synthesis of conjugated poly(arylene Iminophosphorane) and metallopolymers

Polymer 4aa

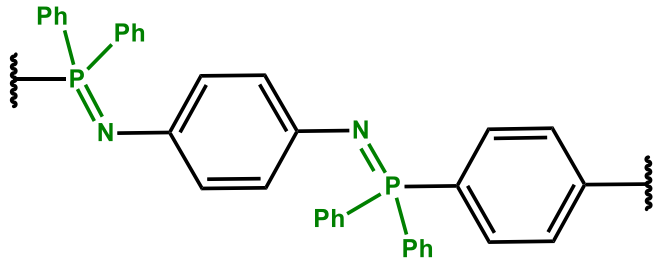

4aa

To a solution of **2a** (97 mg, 0.6 mmol) in 20 ml of DMF, **3a** (268 mg, 0.6 mmol) was added under constant stirring. The dry solvent was purged with argon prior to the addition of **3a**. Within a few minutes, the polymer precipitated. The precipitated product was filtered off and washed with the reaction solvents several times and finally with acetone. Polymers were dried under reduced pressure.

Yield: 99 % (330 mg)

^{13}C CP/MAS NMR

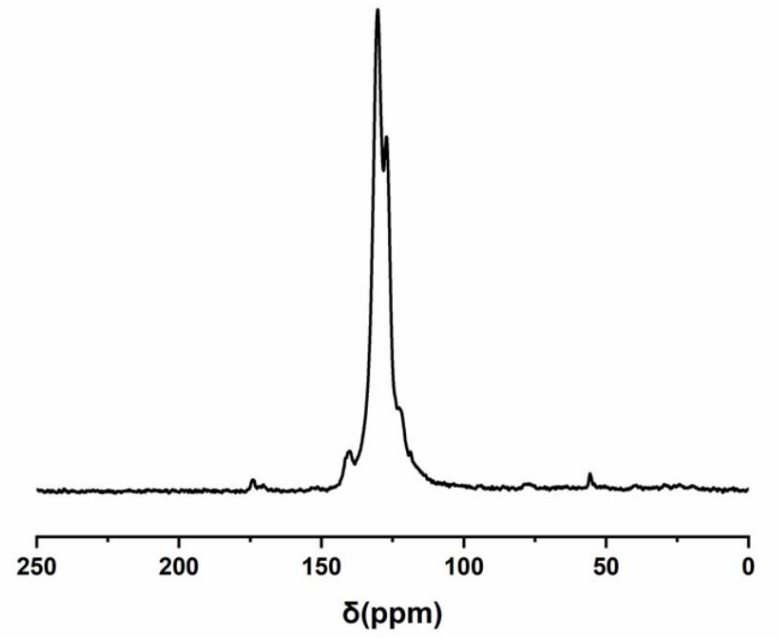

^{13}C CP/MAS NMR (400 MHz): δ 140.10, 130.19, 127.13.

^{31}P CP/MAS NMR

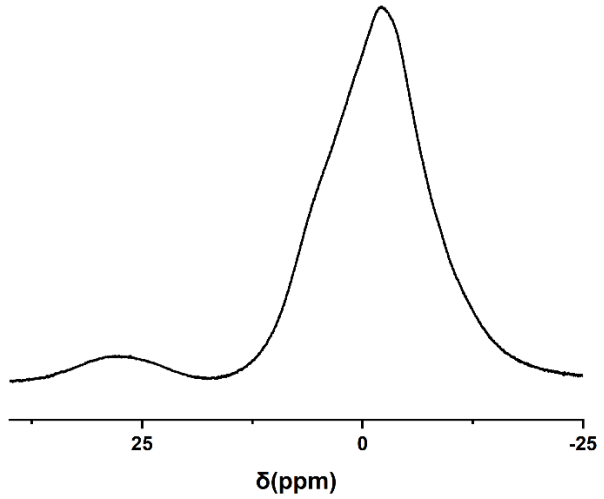

^{31}P CP/MAS NMR (400 MHz): δ 26.5, - 2.2.

FTIR

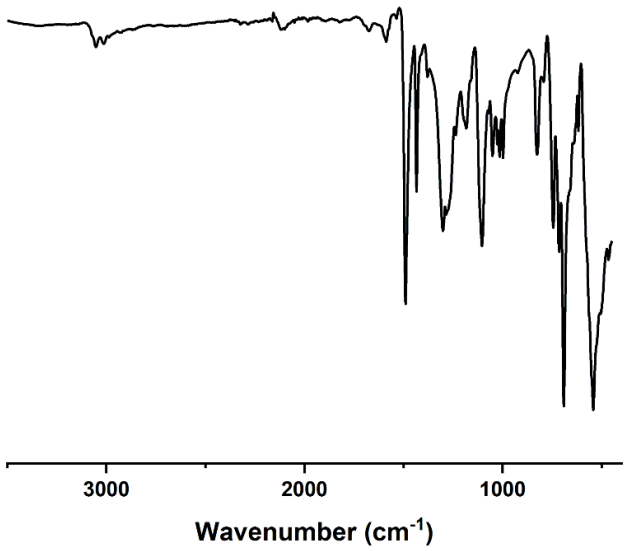

FT-IR (ATR): ν_{max} 3053, 3013, 1489, 1434, 1305, 1274, 1185, 1107, 1049, 1016, 999, 823, 746, 712, 692, 542 cm^{-1}.

Elemental analysis

Element	Experimental (%)	Calculated (%)
C	75.8	78.5
H	5.2	5.1
N	5.1	5.1
S	/	/

Polymer 4ba

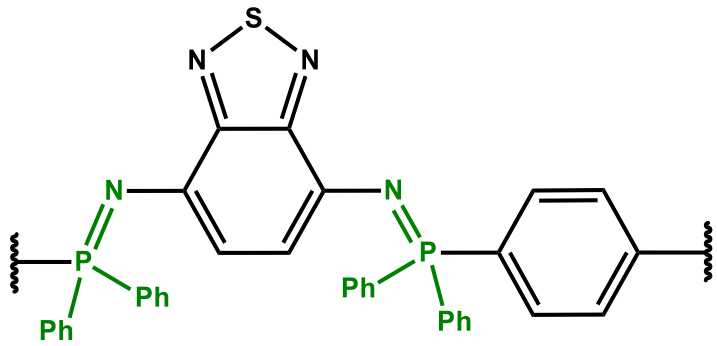

4ba

To a solution of **2b** (131 mg, 0.6 mmol) in DMF (20 ml), **3a** (0.6 mmol, 270 mg) was added under stirring. The dry solvent was purged with argon prior to the addition of **3a**. After a few seconds N_2 started evolving, and the reaction mixture was left overnight to ensure reaction completion. The dark violet polymer was filtered off and washed with DMF, toluene, and finally acetone. The polymer was dried under reduced pressure.

Yield: 99 % (365 mg)

^{13}C CP/MAS NMR

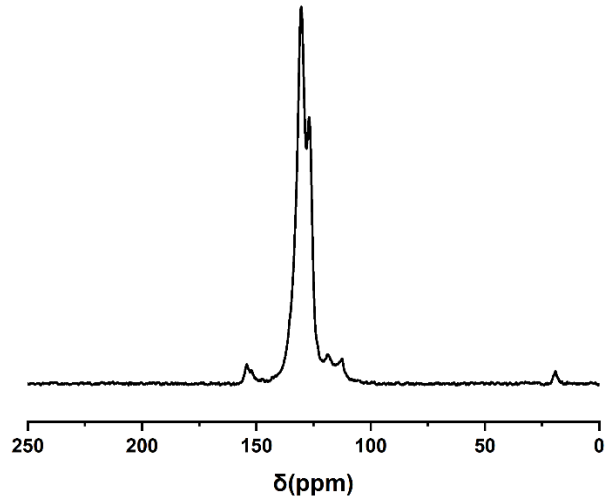

^{13}C CP/MAS NMR (400 MHz): δ 153.98, 130.26, 126.78, 118.92, 112.28.

^{31}P CP/MAS NMR

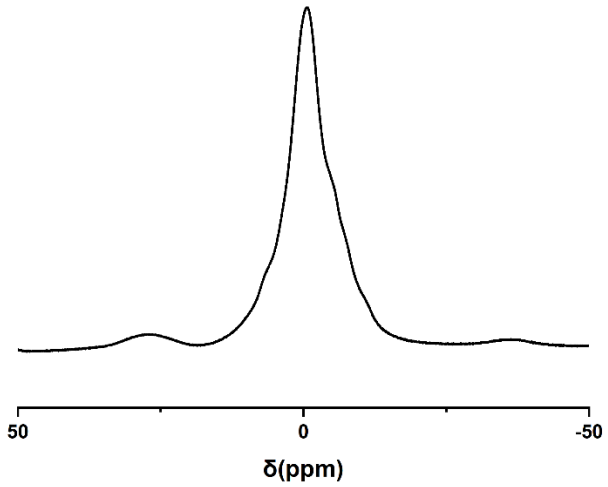

^{31}P CP/MAS NMR (400 MHz): δ 26.38, - 0.60.

FTIR

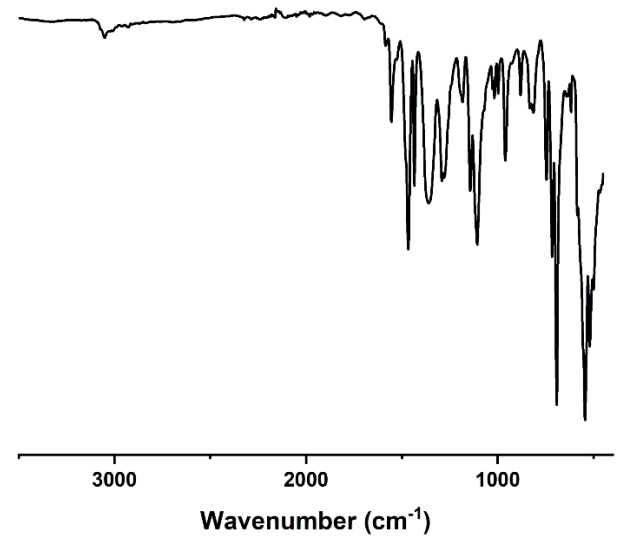

FT-IR (ATR): ν_{max} 3050, 1554, 1468, 1436, 1361, 1291, 1276, 1184, 1144, 1105, 1019, 999, 962, 880, 833, 815, 745, 717, 692, 545, 518 cm^{-1}.

Elemental analysis

Element	Experimental (%)	Calculated (%)
C	70.6	71.0
H	4.8	4.3
N	7.7	9.2
S	4.5	5.3

Polymer 4ca

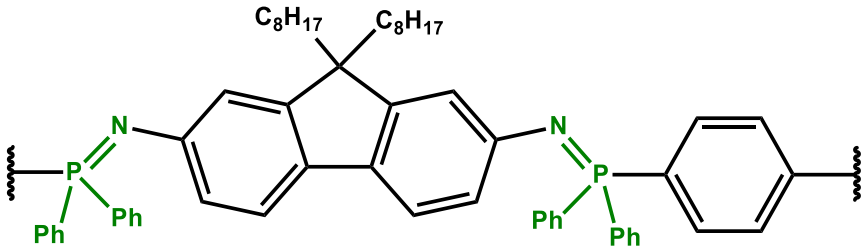

4ca

To a solution of **2c** (283 mg, 0.6 mmol) in DMF (20 ml), **3a** (270 mg, 0.6 mmol) was added under constant stirring. The dry solvent was purged with argon prior to the addition of **3a**. The reaction proceeded rather slowly without any visual evolution of nitrogen and was left for 24 h at room temperature. The reaction mixture was diluted with chloroform (30 ml), and extraction with water was performed to remove DMF. Chloroform was then evaporated under reduced pressure to yield polymer, which was washed with a water/ethanol (1:1) mixture and dried under reduced pressure.

Yield: 92 % (when extracted with chloroform; 492 mg) or 99 % (by azeotropic evaporation of DMF under reduced pressure; 523 mg)

^{13}C CP/MAS NMR

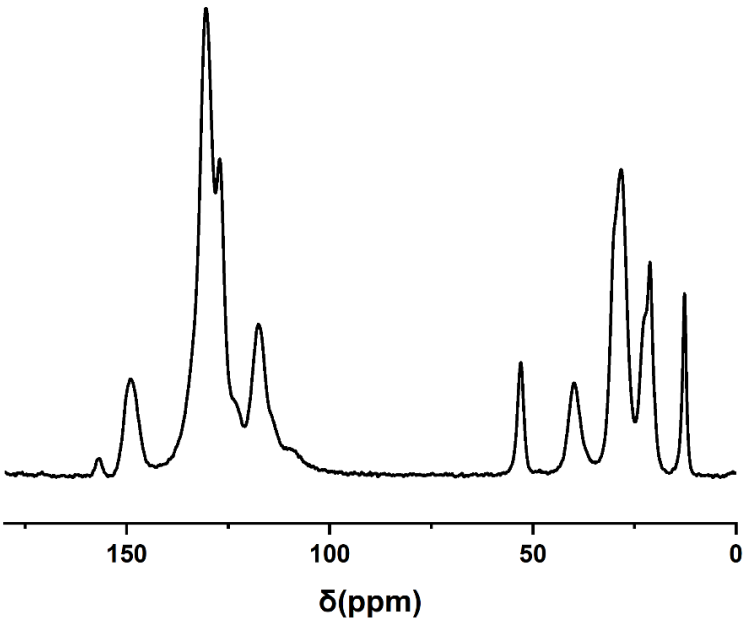

^{13}C CP/MAS NMR (400 MHz): δ 156.62, 149.06, 130.50, 127.08, 117.64, 53.00, 39.66, 28.45, 21.13, 12.63.

^{31}P CP/MAS NMR

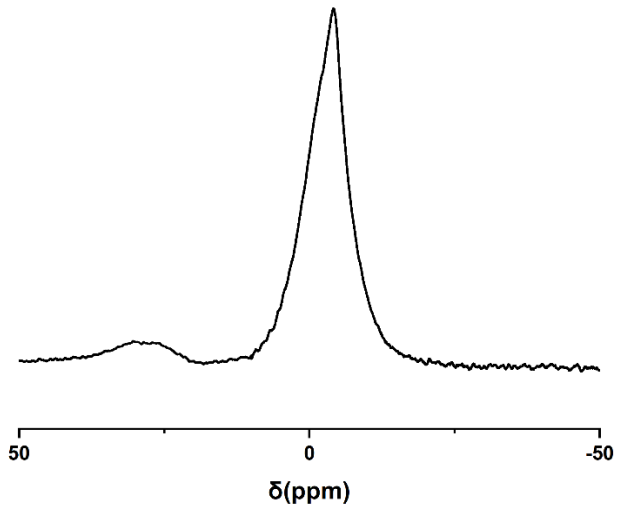

^{31}P CP/MAS NMR (400 MHz): δ 26.32, - 4.1.

FTIR

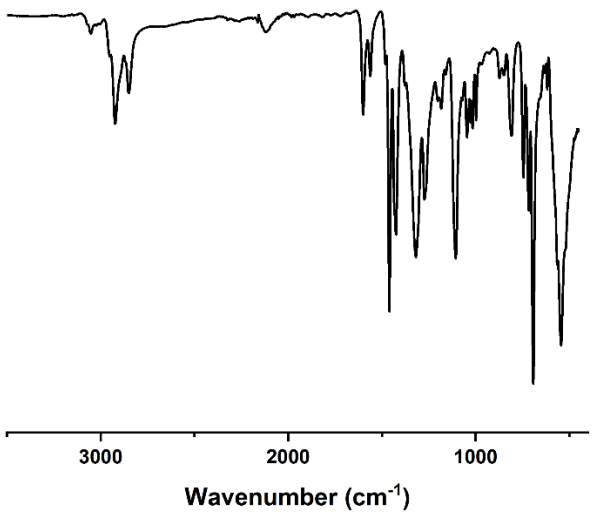

FT-IR (ATR): ν_{max} 3047, 2924, 2848, 2115 (R-N_3), 1602, 1560, 1460, 1423, 1319, 1269, 1180, 1105, 1046, 1026, 1016, 997, 811, 744, 715, 693, 564, 546 cm^{-1}.

Elemental analysis

Element	Experimental (%)	Calculated (%)
C	76.6	81.2
H	6.9	7.5
N	4.8	3.3
S	/	/

Polymer 4ea

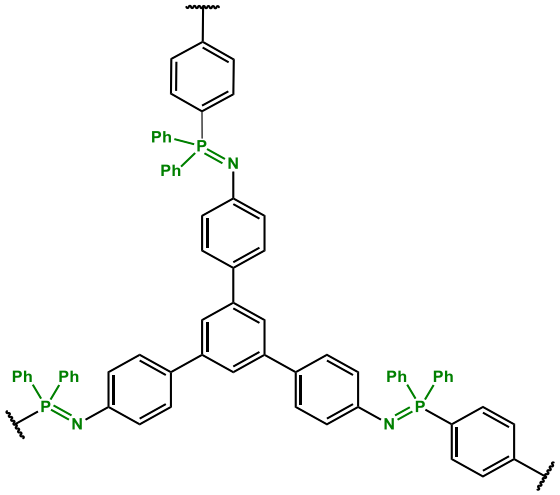

4ea

To a solution of **2e** (286 mg, 0.67 mmol) in DMF (20 ml), **3a** (446 mg, 1 mmol) was added under constant stirring. The dry solvent was purged with argon prior to the addition of **3a.** The reaction proceeded for 4 hours, and the precipitated polymer was washed with DMF, toluene, and acetone. The polymer was dried under reduced pressure.

Yield: 90 % (607 mg)

^{13}C CP/MAS NMR

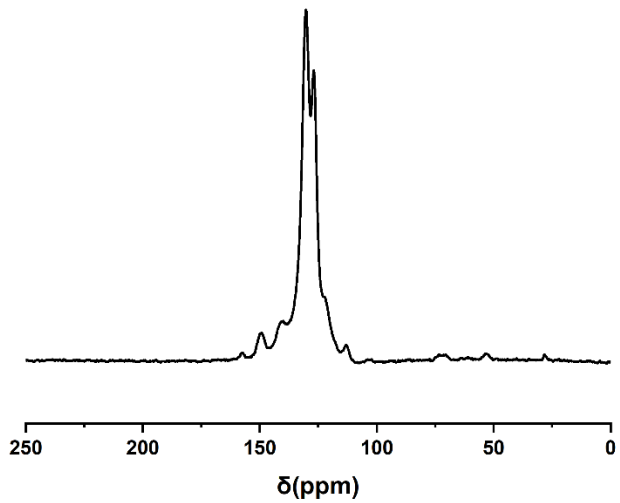

^{13}C CP/MAS NMR (400 MHz): δ 157.43, 149.64, 130.3, 126.8, 122.39, 133.13.

^{31}P CP/MAS NMR

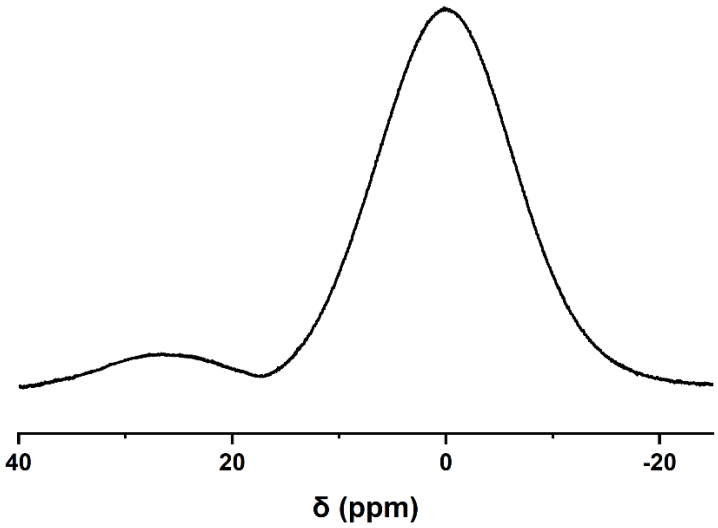

^{31}P CP/MAS NMR (400 MHz): δ 26.06, - 0.36.

FTIR

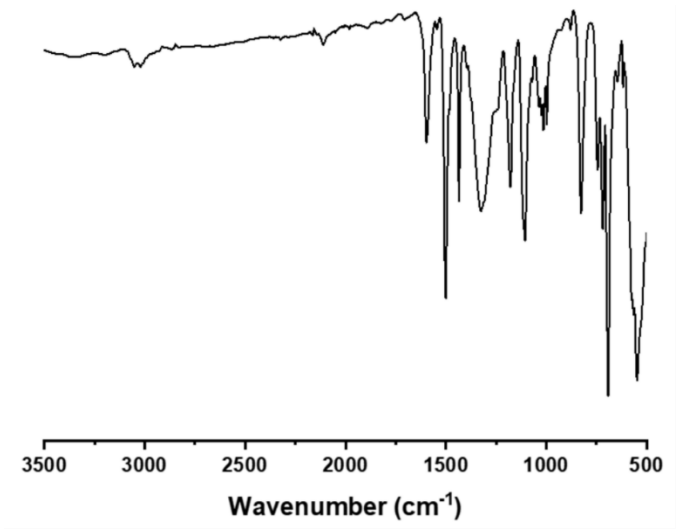

FT-IR (ATR): ν_{max} 3042, 3045, 1594, 2114 (R-N_3- residual), 1503, 1436, 1319, 1177, 1105, 1017, 825, 743, 718, 693, 552 cm^{-1}.

Elemental analysis

Element	Experimental (%)	Calculated (%)
C	75.6	82.1
H	4.8	5.1
N	3.4	4.0
S	/	/

Polymer 4ab

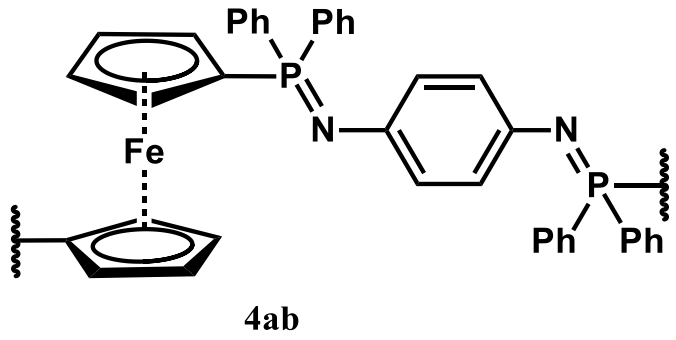

4ab

To a solution of **2a** (80 mg, 0.5 mmol) in hot DMF (80 °C, 10 ml), **3b** (277 mg, 0.5 mmol) was added under constant stirring. The dry solvent was purged with argon prior to the addition of **3b.** The reaction proceeded rapidly, and the precipitated polymer was washed with DMF and acetone. The polymer was dried under reduced pressure.

Yield: 93 % (305 mg)

^{13}C CP/MAS NMR

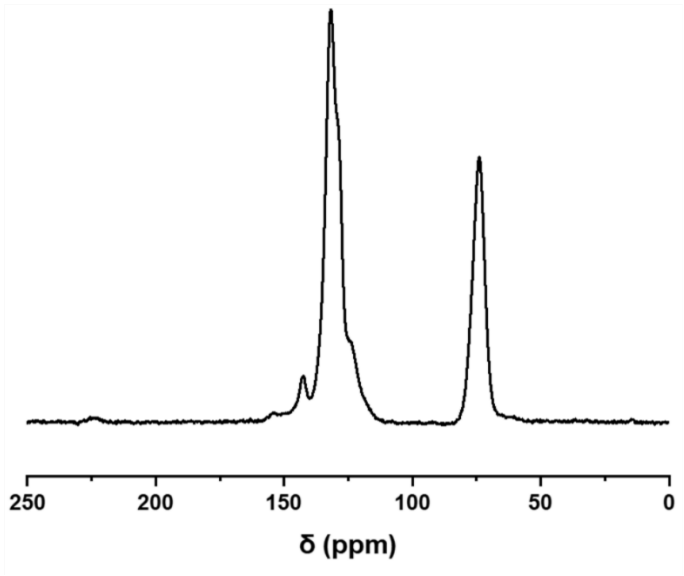

^{13}C CP/MAS NMR (400 MHz): δ 142.97, 131.77, 74.00.

^{31}P CP/MAS NMR

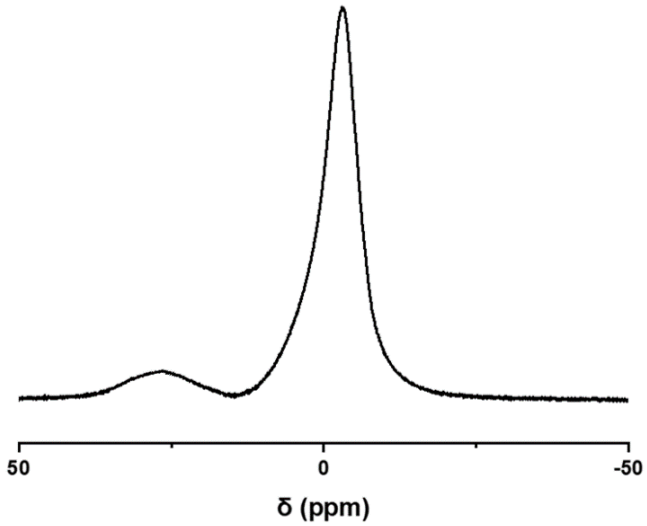

^{31}P CP/MAS NMR (400 MHz): δ 27.02, -2.94.

FTIR

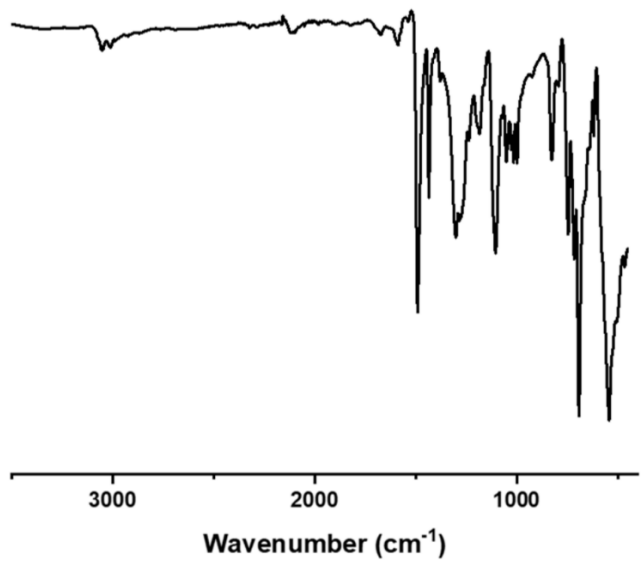

FT-IR (ATR): ν_{max} 3057, 3013, 1489, 1434, 1297, 1197, 1108, 1047, 829, 746, 717, 691, 541 cm^{-1}.

Elemental analysis

Element	Experimental (%)	Calculated (%)
C	76.6	81.2
H	6.9	7.7
N	4.8	3.2
S	/	/

Polymer 4eb

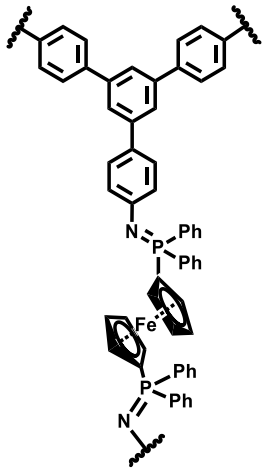

4eb

To a solution of **2e** (28.6 mg, 0.066 mmol) in hot DMF (80 °C, 10 ml), **3b** (55.4 mg, 0.1 mmol) was added under constant stirring. The solvent was purged with argon prior to the addition of **3b.** The reaction proceeded rapidly, and the precipitated polymer was washed with DMF and acetone. The polymer was dried under reduced pressure.

Yield: 88 % (69 mg)

^{13}C CP/MAS NMR

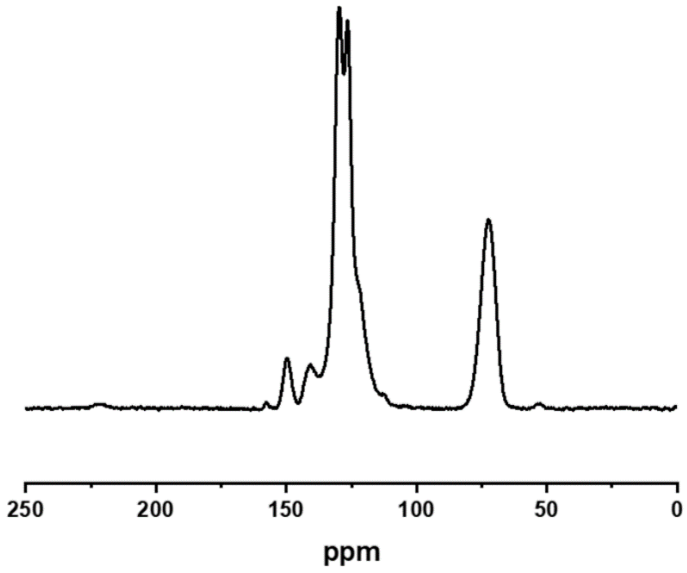

^{13}C CP/MAS NMR (400 MHz): δ 149.70, 140.77, 129.65, 126.56, 72.42.

^{31}P CP/MAS

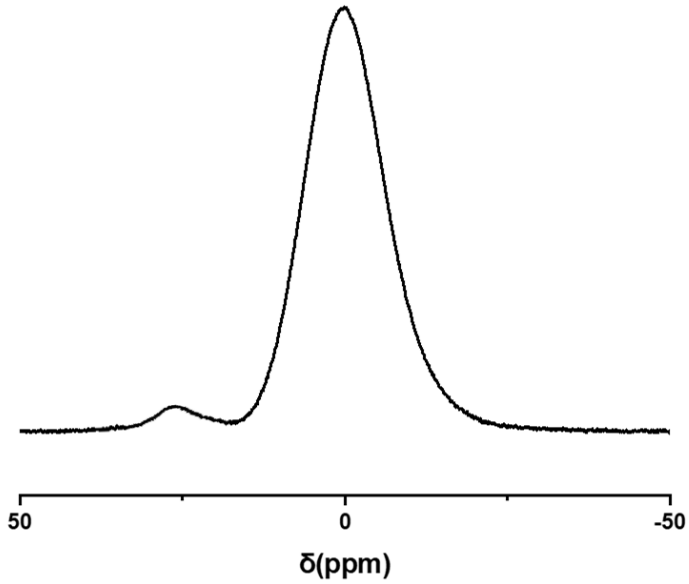

^{31}P CP/MAS NMR (400 MHz): δ 26.88, -0.11.

FTIR

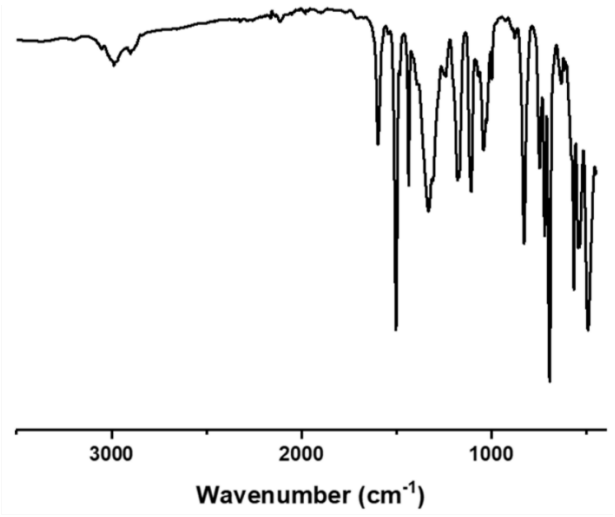

FT-IR (ATR): ν_{max} 2992, 2892, 1597, 1504, 1436, 1328, 1170, 1110, 1045, 830, 744, 719, 695, 631, 567, 538, 491cm^{-1}.

Elemental analysis

Element	Experimental (%)	Calculated (%)
C	76.2	75.9
H	6.6	6.4
N	3.86	3.0
S	/	/

IV. Effect of Moisture

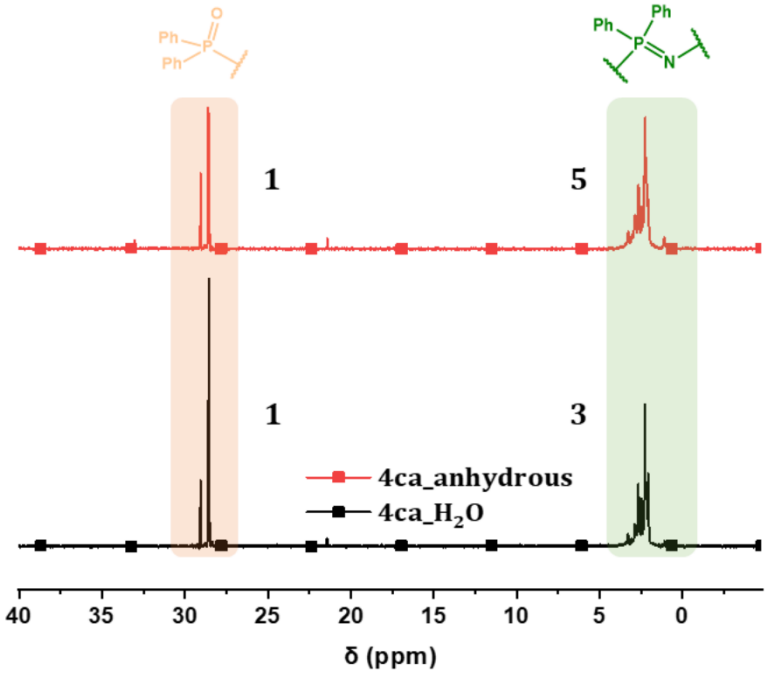

Figure S2. ^{31}P NMR of polymer 4ca synthesized in anhydrous (red) and humid (black) conditions.

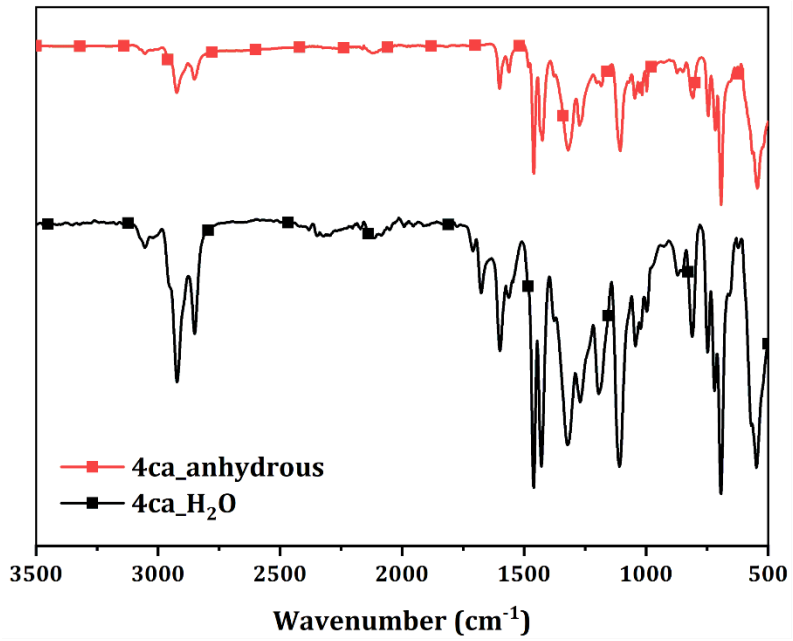

Figure S3. FTIR spectra of polymer 4ca synthesized in anhydrous and moist conditions.

V. Effect of Atmosphere (^{31}P CP/MAS NMR)

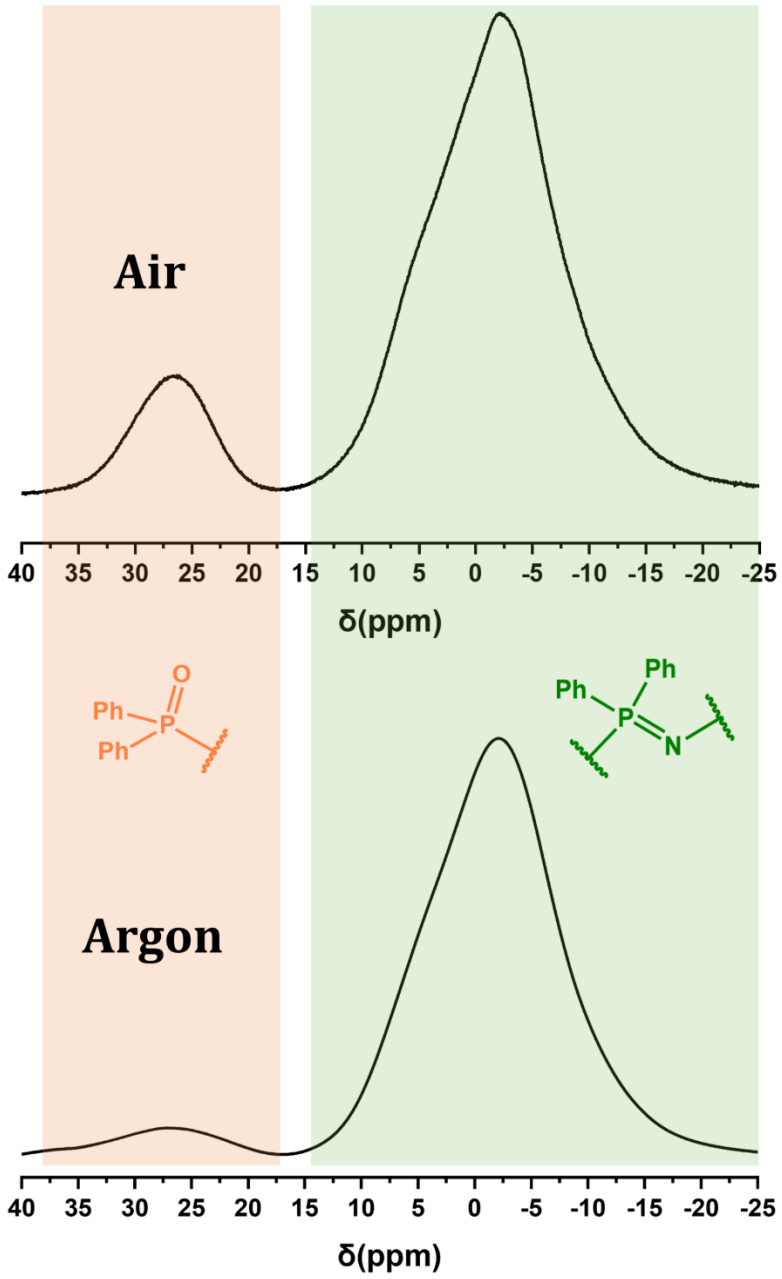

Figure S4. Atmospheric effect on the oxidation of phosphine end-groups in case of polymer **4ca**.

VI. SEC analysis

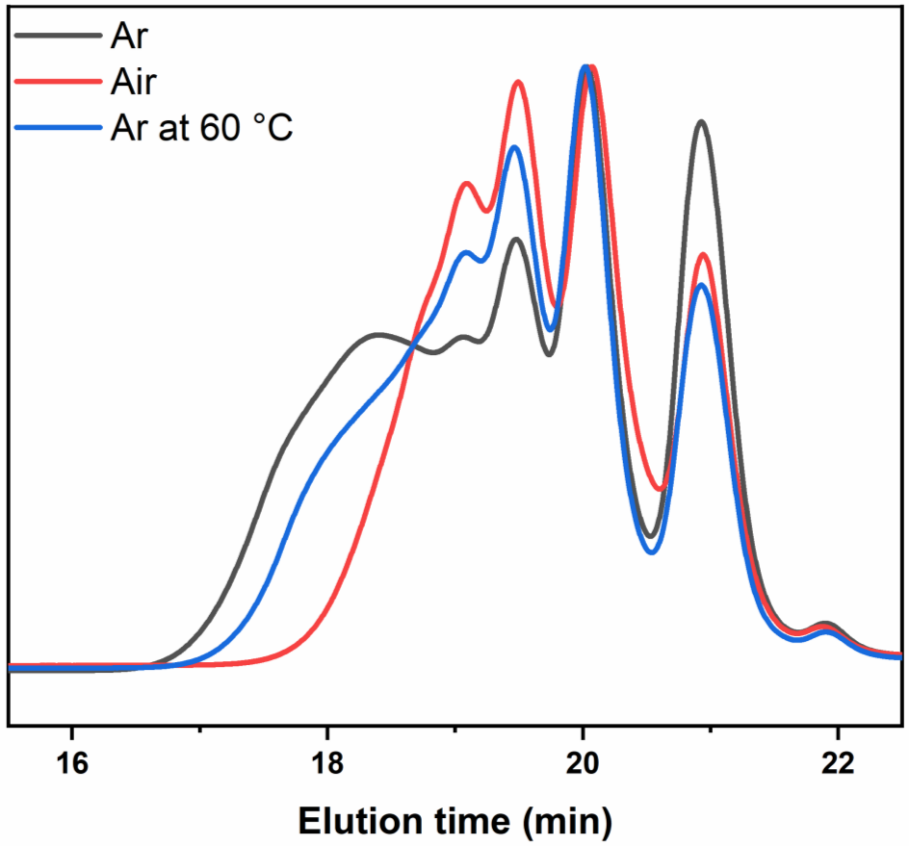

Figure S5. Overlay of SEC chromatograms of poly(arylene Iminophosphorane) **4ca** prepared in DMF under different atmospheres, light conditions, and temperatures (Table 1, entries 2, 4, and 6).

VII. MALDI ToF analysis

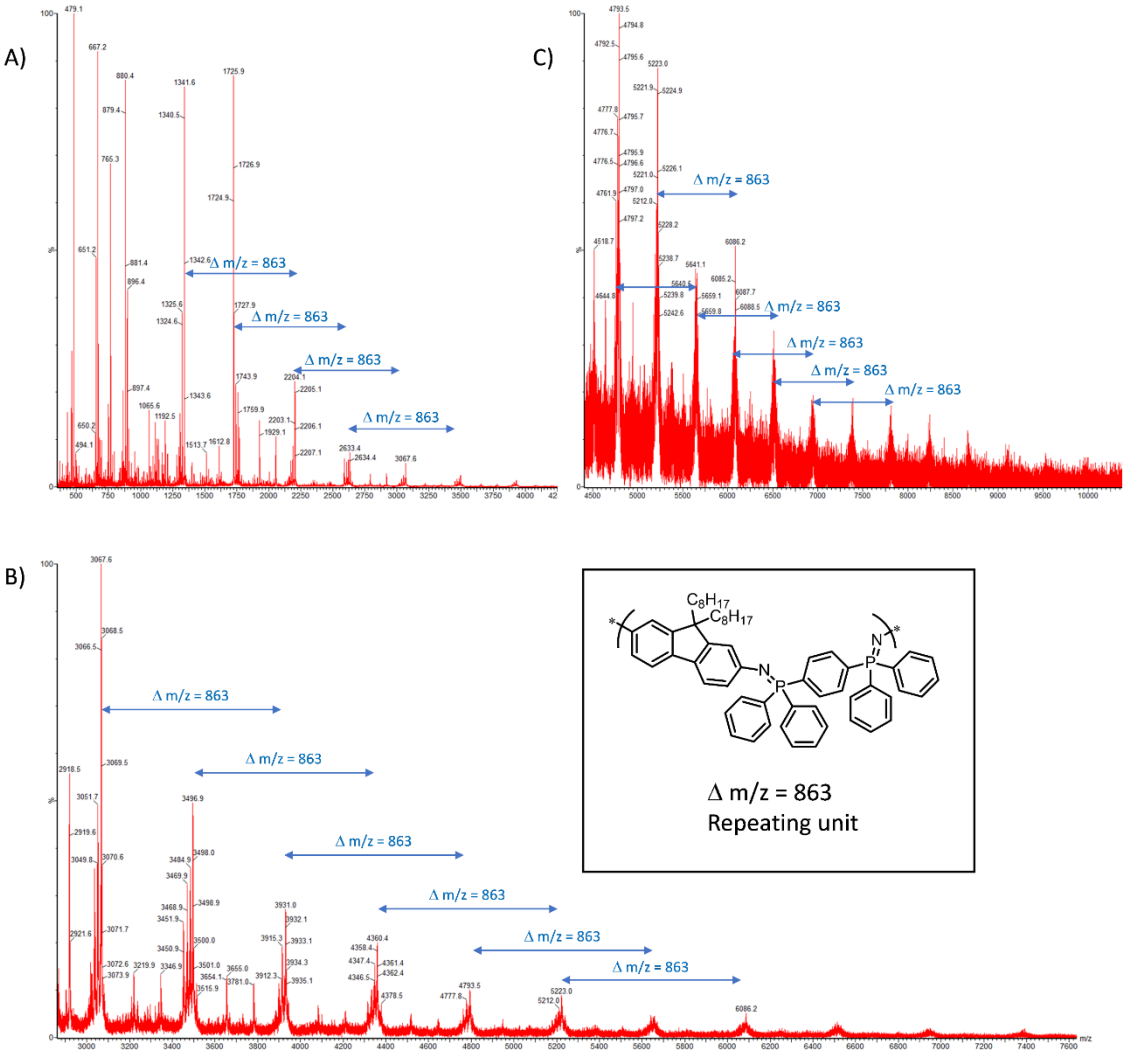

Figure S6. MALDI-ToF spectrum of the poly(arylene Iminophosphorane) **4ca**. Magnification between 400-4000 m/z (A), 2900-7600 m/z (B) and 4500-10500 m/z (C).

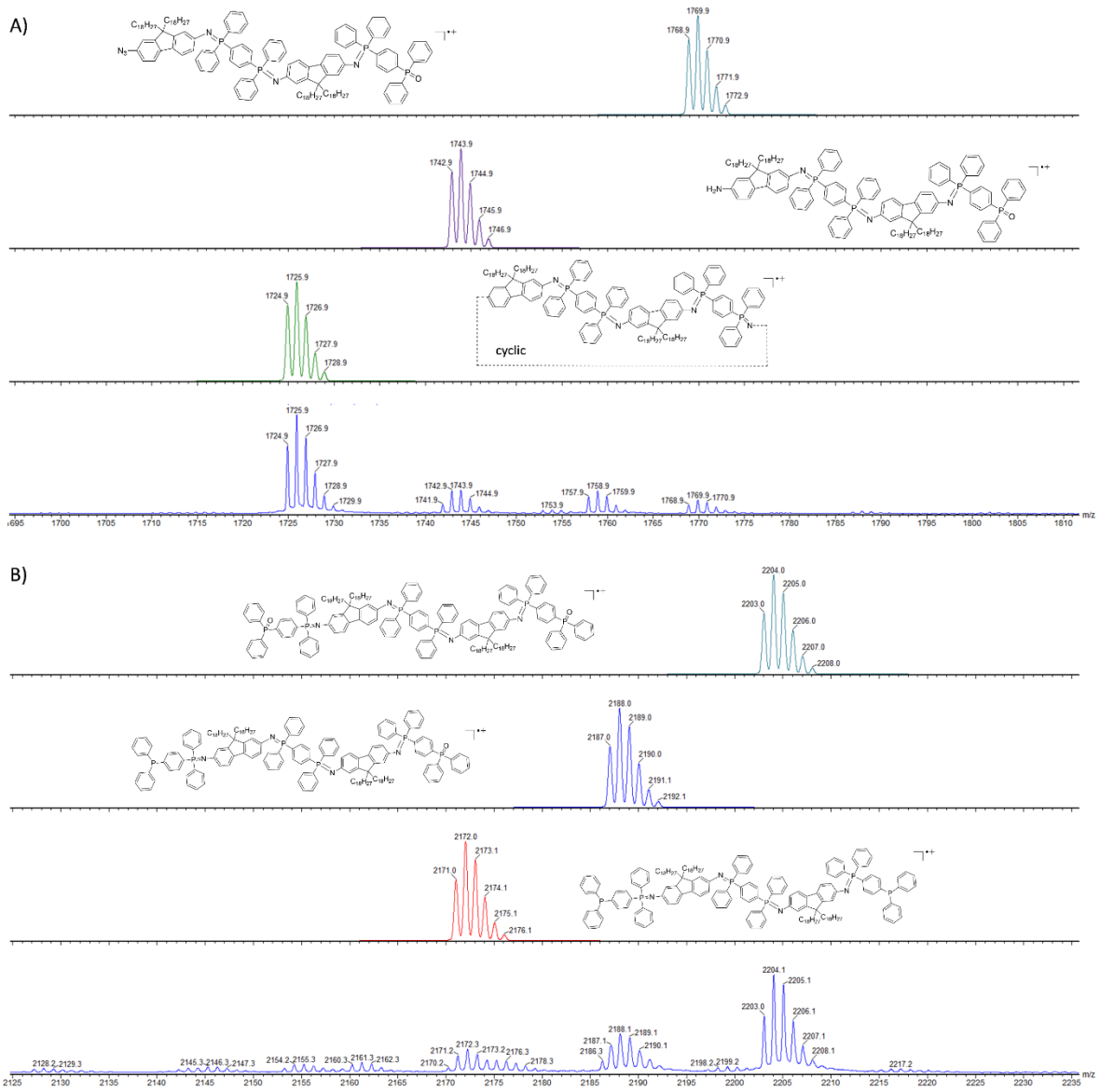

Figure S7. Comparison between the theoretical and experimental isotopic distribution for the MALDI-ToF spectrum of the poly(arylene Iminophosphorane) **4ca**. Magnification between 1700-1810 m/z (A) and 2125-2235 m/z (B).

VIII. Investigation of sterical hindrance by ^{31}P NMR

Azide **2d** (20 mg, 0.1 mmol) and phosphine **3a** (66 mg, 0.15 mmol) were reacted in $CDCl_3$ and the reaction was followed by ^{31}P NMR spectroscopy. We can see the gradual disappearance of the phosphine monomer (δ ~ -5 ppm) during the course of the reaction, and total consumption after 24 h (**Figure S8A**). Simultaneously, two new peaks appear, the downfield shifted peak at ~ 1 ppm belonging to the phosphazene linkage, and the upfield shifted peak at ~ -3 ppm, which we assigned to the unreacted phosphine end-groups.

To further test our hypothesis on the photocatalytic oxidation of phosphine groups, we put our NMR tube, with the same sample used for *in situ* ^{31}P NMR, on a window shelf for several days. The tube was opened once per day for a few seconds to enable oxygen access. Due to the presence of oxygen and natural light coming through the window, we can observe the oxidation of phosphine end-groups (peak at ~ -3 ppm decreasing over 72 h) to phosphine oxide end-groups (peak at ~ 29 ppm increasing over 72 h) (**Figure S8B**). Whereas the same sample when in NMR (dark) for 24 h showed a neglectable amount of phosphine oxide end-groups. This further supports our hypothesis on the photocatalytic oxidation of phosphine end-groups.

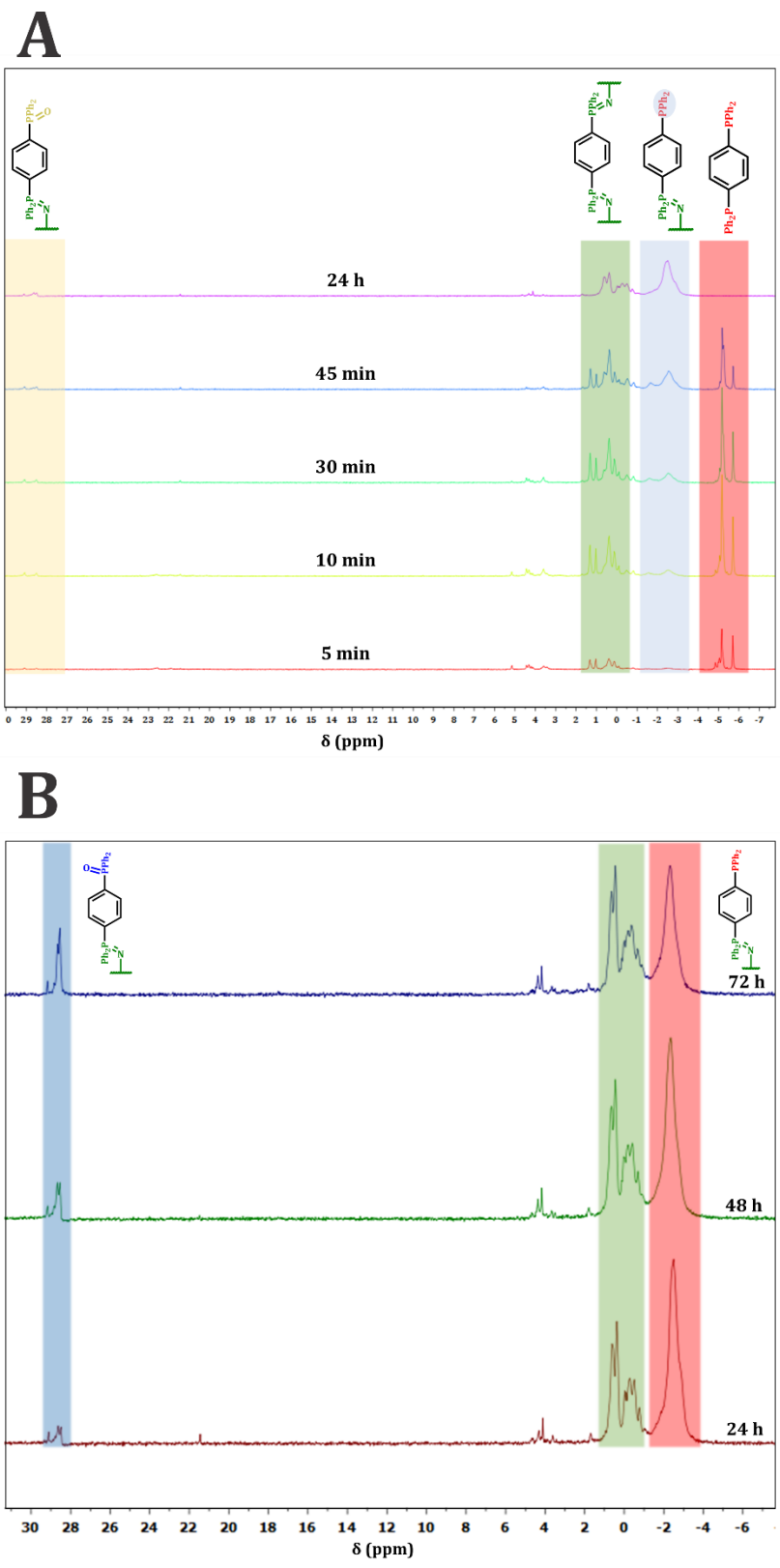

Figure S8. *In situ* ^{31}P NMR spectroscopy of the reaction between **2d** and **3a** (A) (since the NMR tube was in the spectrometer for 24 h there was no access to light), and the same sample was exposed to sunlight for several days (B).

IX. IR spectroscopy

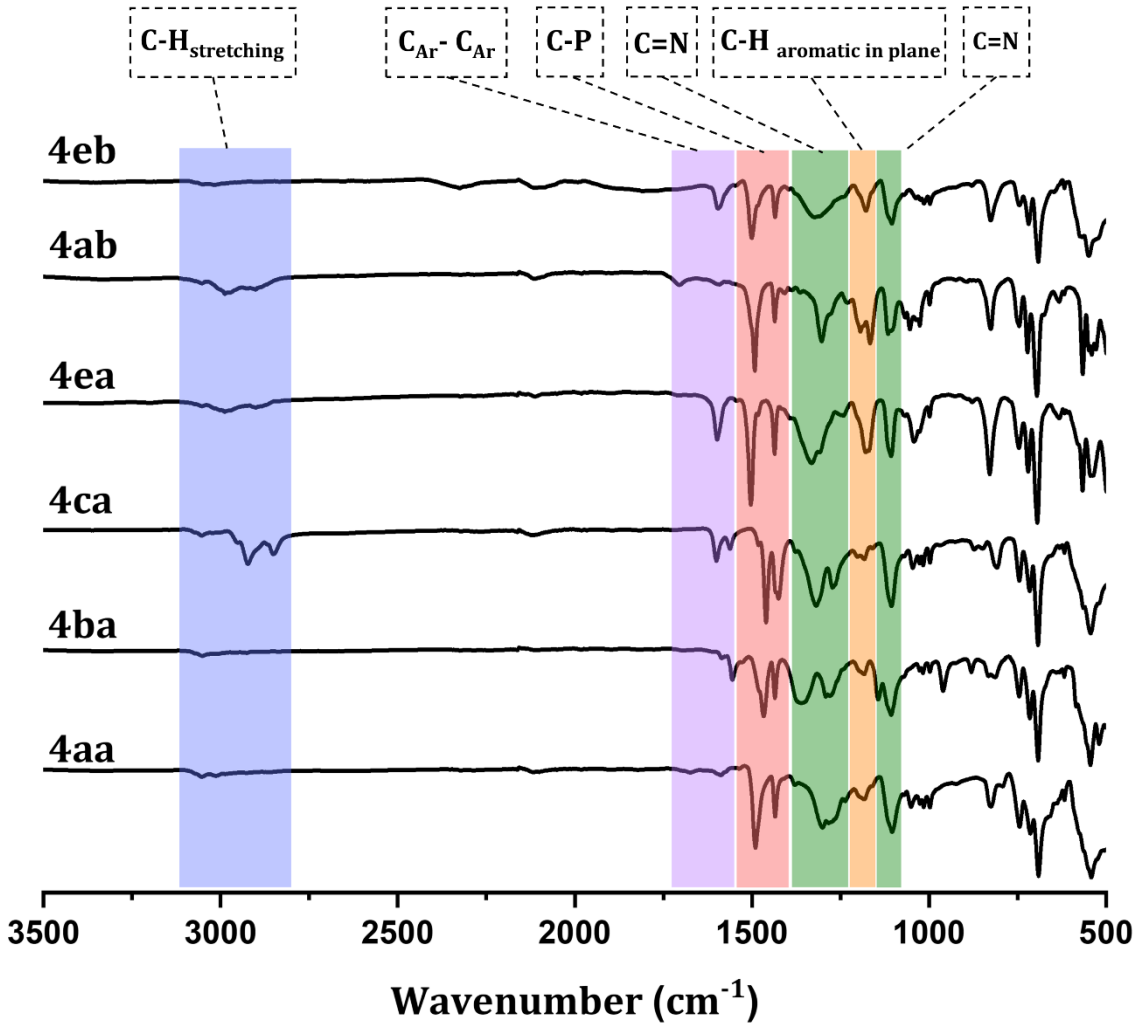

Figure S9. Assignation of characteristic peaks in poly(arylene iminophosphorane) FTIR spectra.

X. Thermal analysis of poly(arylene iminophosphorane)

Table S1. Thermal properties of PAIPs.

Sample	$T_{0.1}$, [°C[a]]		T_{max}, [°C[b]]		T_g, [°C]
	N_2	Air	N_2	Air	
4aa	403	426	482	444	132
4ba	381	395	462	545	166
4ca	407	413	449	492	81
4ea	403	475	514	513	182
4ab	356	412	391	548	146
4eb	361	413	360	443	188

[a] Temperature at 10% mass loss. [b]Temperature at maximum mass loss rate retrieved from dTG curves.

TGA - Thermal stability

Main manuscript **Figure 5B**

Temperature program: 25 °C – 900 °C; Heating ramp: 10 °C/min, N_2 atmosphere (20 ml/min).

TGA - Oxidative stability

Temperature program: 25 °C – 900 °C; Heating ramp: 10 °C/min, air atmosphere (20 ml/min).

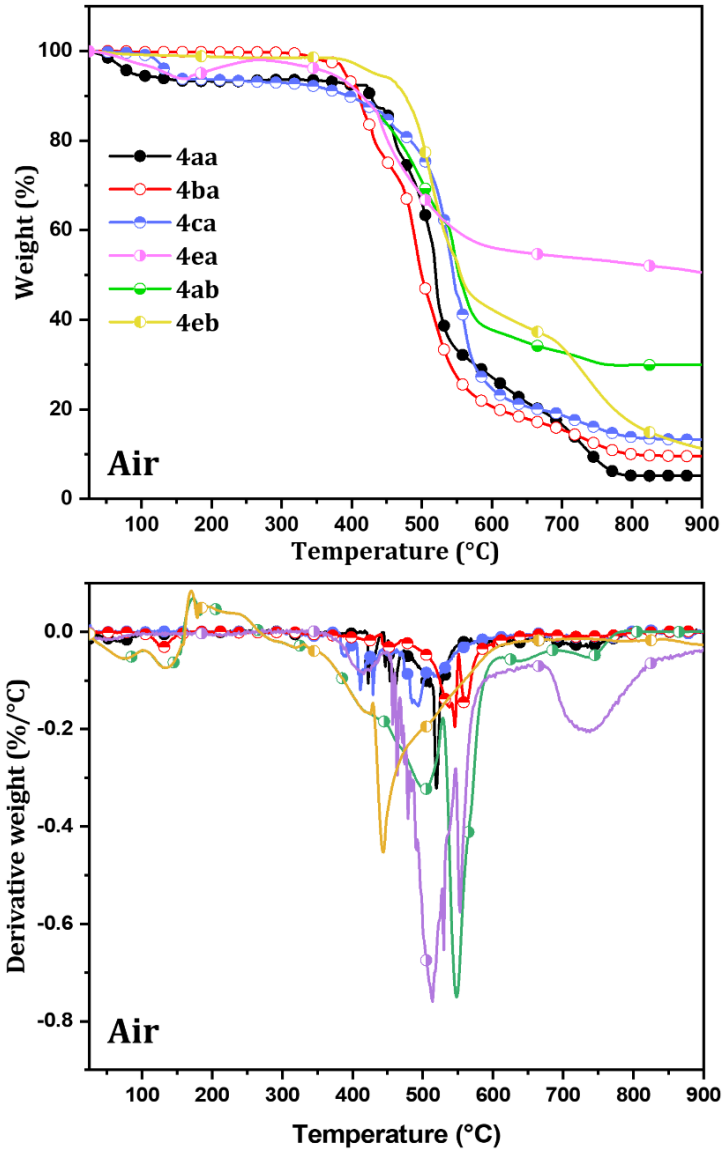

Figure S10. Dynamic TGA thermograms of PAIP polymers in air atmosphere.

TGA- isothermal test

Main manuscript **Figure 5D**

Temperature program: 25 °C – 400 °C; Heating ramp: 10 °C/min, isothermal holding at 400 °C for 30 minutes, air atmosphere (20 ml/min).

DSC

DSC thermograms of PAIPs are shown in Figure S11. PAIPs exhibit a T_g between 81 and 188 °C (Table S1), which is significantly higher than the values reported in the literature for polyphosphazenes, ranging between -60 and 40 °C.[64] The higher T_g suggests that molecular mobility is restricted in PAIPs, probably due to the incorporation of aromatic fragments between phosphazene linkages on the one hand and crosslinking nodes (e.g., **2e**) on the other into the macromolecular network, which is responsible for the extensive π-π interactions between polymer chains and the stiffening of the macromolecular network, affecting the T_g. For example, in polymer **4ba**, which contains the benzothiadiazole motif with a planar structure, the π-π stacking between the chains is correspondingly stronger, and thus the T_g is higher than in polymer **4ca**, which contains the 9,9-dioctylfluorene core with the intertwined alkyl chains that prevent good π-π stacking. In the case of **4ea** and **4eb** additionally to the π-π interactions, the 1,3,5-tris(4- azidophenyl)benzene (**2e**) acts as a crosslinking node, driving up the T_g even further to 182 and 188 °C, respectively.

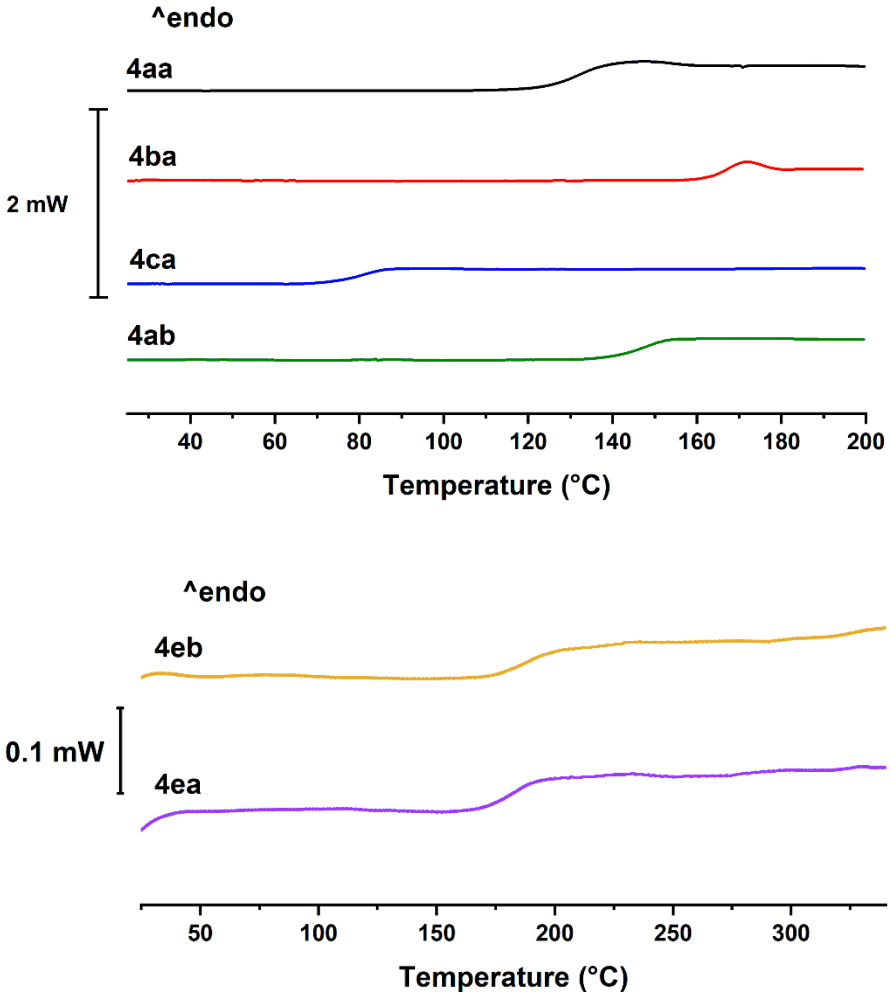

Figure S11. DSC thermograms of poly(arylene iminophosphorane).

Temperature program:

i) linear polymers: -80 – 200 °C; Heating ramp: 10 °C/min, N_2 atmosphere (20 ml/min).

ii) crosslinked polymers: 0 – 400 °C; Heating ramp: 10 °C/min, N_2 atmosphere (20 ml/min).

XI. Optoelectronic properties of poly(arylene iminophosphorane)

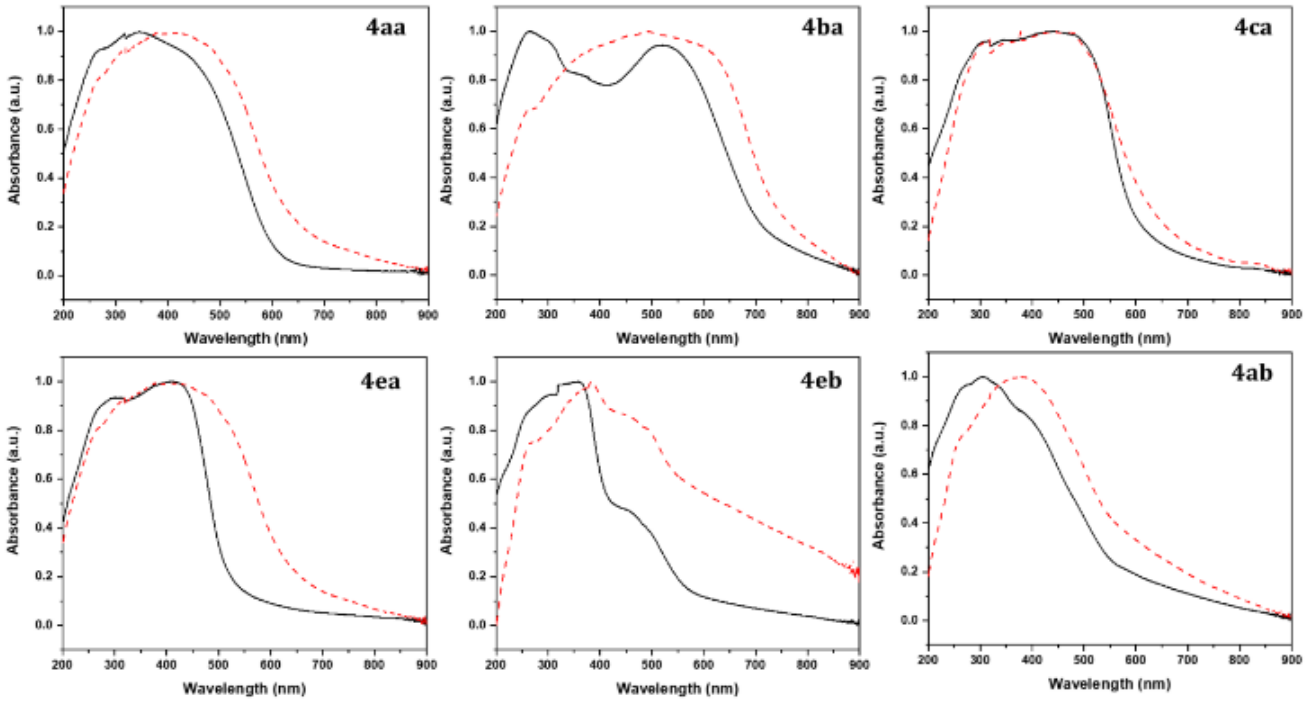

Figure S12. UV-Vis-DRS spectra of polymers before (—) and after (---) thermal annealing.

XII. Photocatalytic tests

The reaction between the bis-alkylated fluorene diazide (**2c**; 80 mg, 0.17 mmol) and 1,4-bis(diphenylphosphanyl)benzene (**3a**; 76 mg, 0.17 mmol) to form **4ca**, was used as the model reaction for the mechanistic investigation of phosphine oxide end-group formation. A series of experiments conducted under light illumination, in the dark, under argon atmosphere, and in the presence of quenchers (DABCO and HQ) gave an insight into the oxidation mechanism of the phosphine groups. ^{31}P NMR experiments were performed in a quantitative manner, and the ratio between the integral values for the phosphorous in the phosphazene linkage and in the phosphine-oxide gave information about the extent of oxidation.

General setup:

The reactions were carried out in a double neck round bottom flask equipped with a dropping funnel on the wider neck and a septum stopper on the smaller neck. Azide **2c** was dissolved in 10 ml of dry DMF and poured into the dropping funnel, which was also sealed with a septum stopper. Phosphine **3a** was dissolved in 10 ml of dry DMF and poured into the double neck round bottom flask (**Scheme 1A**). In cases where an inert atmosphere was desired, argon was supplied into both solutions, i.e., in the dropping funnel and double neck round bottom flask (**Scheme 1B**) for 2 h prior to the reaction. In the case of experiments with light illumination, the KL 1600 LED light source was used (**Scheme 1C**) whereas in the case of dark experiments, the whole setup was covered in aluminum foil and performed in a dark room.

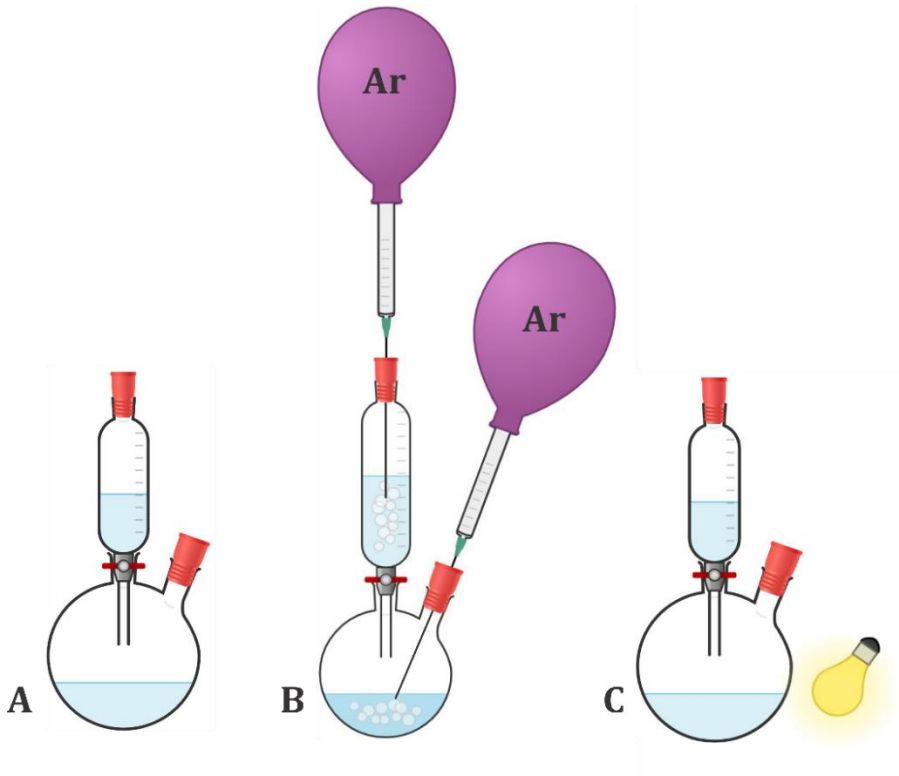

Scheme 1. Glassware setups for reaction under static air atmosphere (A), in case of argon atmosphere (B), and under illumination (C).

The following experiments were performed (main manuscript **Figure 2**):

I) under light illumination and aerified with compressed air (Light & O_2);

The ratio of integrals (1:2) in ^{31}P NMR shows that ~33 % of the phosphine oxidizes during the reaction.

II) under light illumination, aerified with compressed air and the addition of DABCO (1 g);

We observe a slight decrease in the amount of phosphine-oxide end-groups from ~33 % to ~28.5 %*, corresponding to a 14 %** relative decrease in oxidized end-groups. This indicates that the presence of $^1O_2$ is not the main reason for the oxidation process.

III) under light illumination, aerified with compressed air and addition of HQ (1 g);

In this case, a substantial decrease of the phosphine-oxide end-groups from ~33 % to ~14 %* is observed, corresponding to a 57 %** relative decrease in oxidized end-groups. HQ is showcasing the superoxide anion's importance in the phosphine groups' oxidation path.

IV) under light illumination and argon atmosphere;

A significant decrease of the phosphine-oxide end-groups from ~33 % to ~5 % shows that atmospheric oxygen is the main source for ROS generation, hence phosphine oxidation. The residual 5 % is due to the lack of a total inert atmosphere, for which we would need a Schlenk line; however, that would largely complicate the polymerization procedure.

V) in the dark and aerified with compressed air;

A minimal amount of phosphine-oxide end-groups was observed in this case (~4 %), revealing that oxygen and light need to be present for efficient oxidation.

VI) in the dark and under argon atmosphere;

This experiment further confirmed that both inert atmosphere and darkness constrain the oxidation of phosphine groups since we observe only ~3 % of the phosphine oxide end-groups.

*The above relative amount (w; %) of phosphine oxide end-group was calculated by the following equation from the corresponding peak integrals in ^{31}P NMR spectra:

$$w(\text{oxidized phosphine}, \%) = \frac{\int PPh3O}{\sum \int P\ species} \times 100;$$

$\int PPh3O$ - peak integral for phosphorus in the phosphine oxide end-group at ~ 29 ppm;

$\sum \int P\ species$ - the sum of all peak integrals in the ^{31}P NMR spectra.

**The relative decrease (RD) of phosphine oxide end-groups when using a quencher (P_{quench}) compared to the initial experiment conducted at ambient conditions ($P_{ambient}$) was calculated by the following equation:

$$RD\ (\%) = \left(1 - \frac{\int \text{Pquench}}{\int \text{Pambient}}\right) \times 100$$

XIII. Glassy film formation

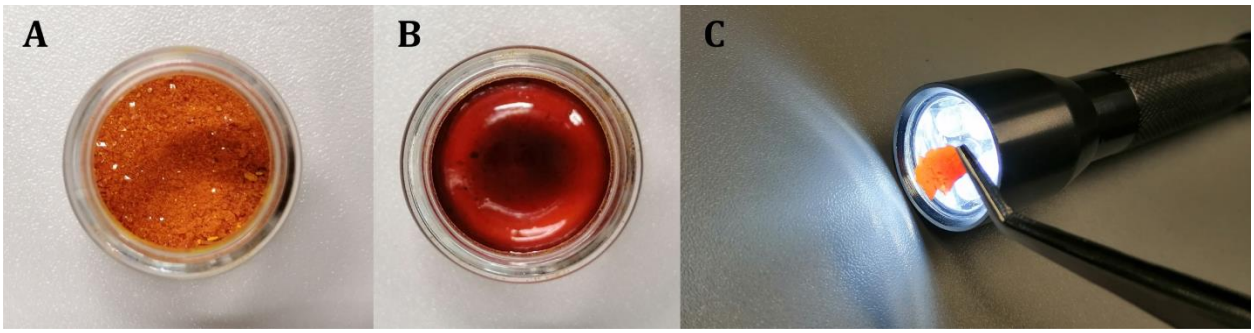

Figure S13. Polymer **4ca**, as an opec powder (A), transforms into a translucent glassy film (B and C) after heating above the glass transition temperature (T_g).

XIII. XRD analysis

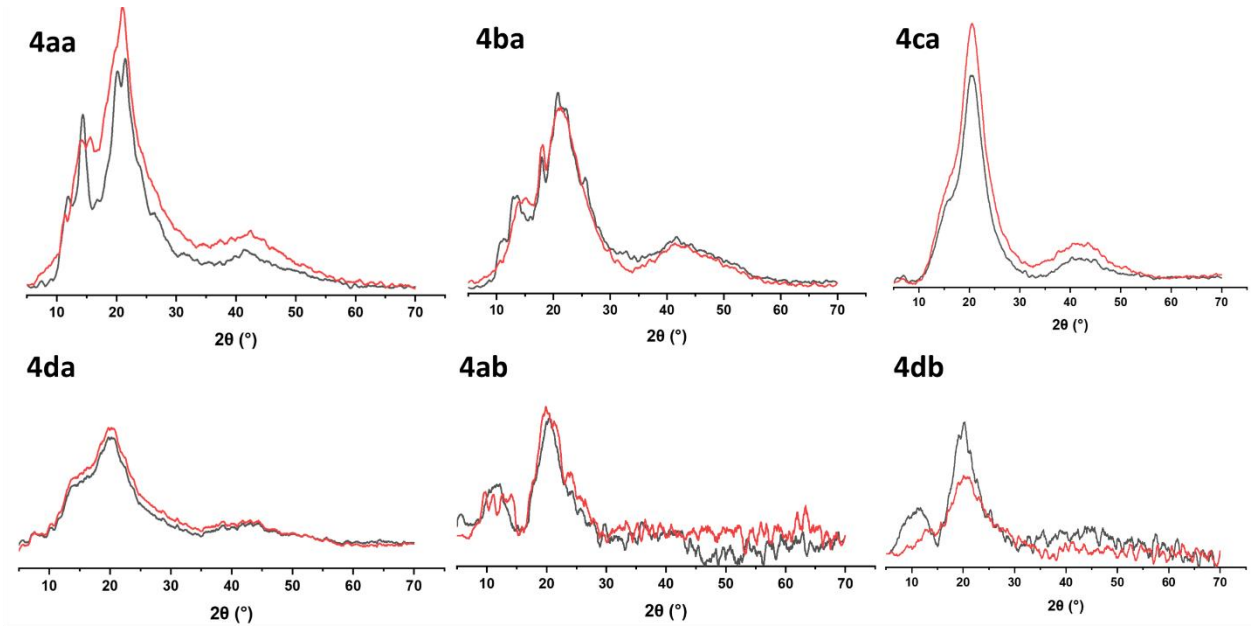

Figure S14. XRD analysis of poly(arylene iminophosphorane) before (—) and after (—) thermal annealing.

XIV. Π-Conjugated polymer and metallopolymer foams

Synthesis of **4ea** foam:

To a solution of **3a** (223 mg, 0.5 mmol) in hot DMF (80 °C, 1 ml) in a glass vial, **2e** (143 mg, 0.33 mmol) was added under constant stirring with a glass spatula. The solvent was purged with argon prior to the addition of **2e**. The reaction proceeded rapidly, and the precipitated polymer foam was washed with DMF and acetone. The polymer was dried under reduced pressure.

Synthesis of **4eb** foam:

To a solution of **3b** (110.8 mg, 0.2 mmol) in hot DMF (80 °C, 2 ml) in a glass vial, **2e** (57 mg, 0.13 mmol) was added under constant stirring with a glass spatula. The solvent was purged with argon prior to the addition of **2e**. The reaction proceeded rapidly, and the precipitated polymer foam was washed with DMF and acetone. The polymer was dried under reduced pressure.

XV. Nitrogen physisorption

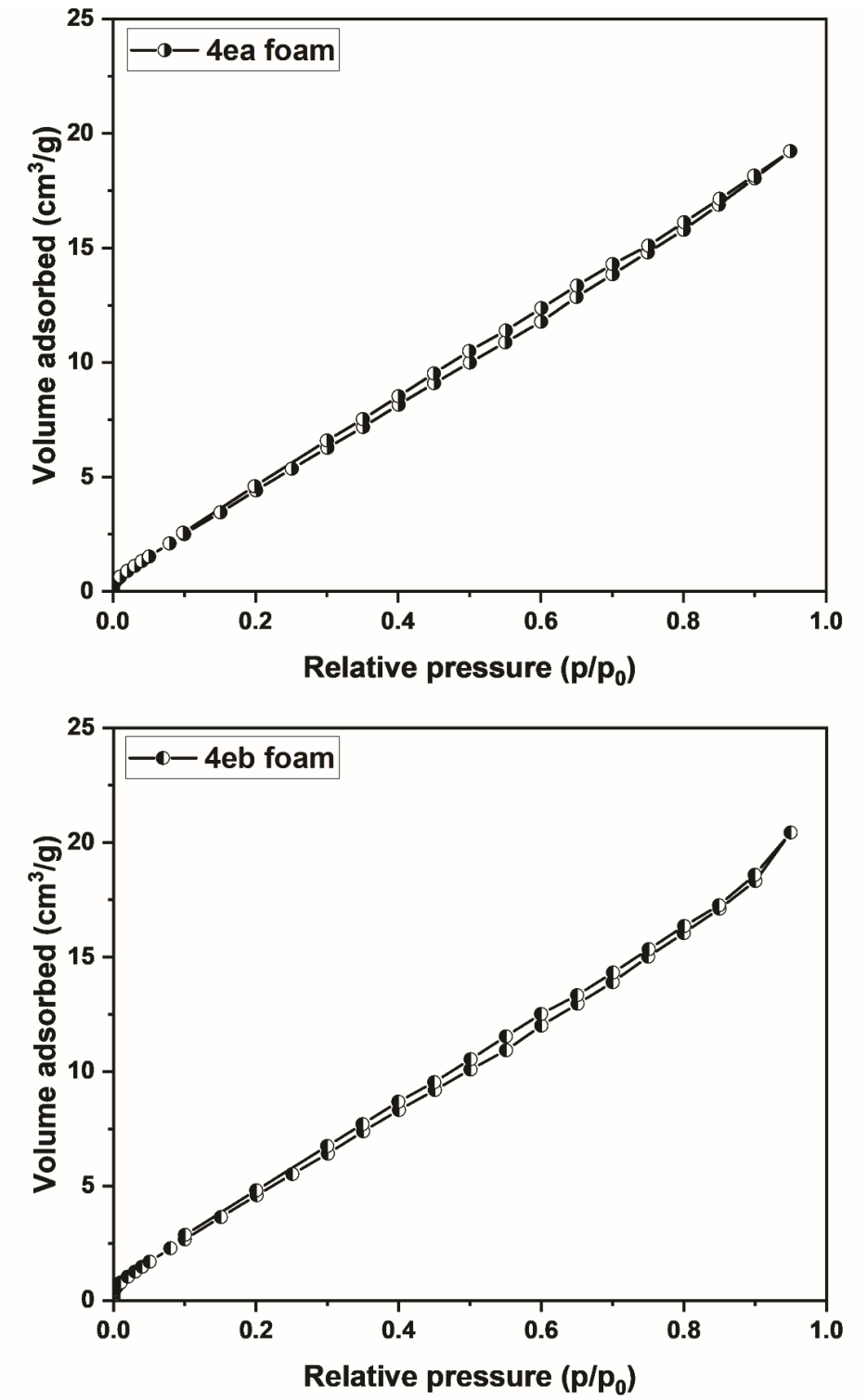

Figure S15. Nitrogen physisorption isotherms for **4ea** and **4eb** foams.

XVI. SEM analysis

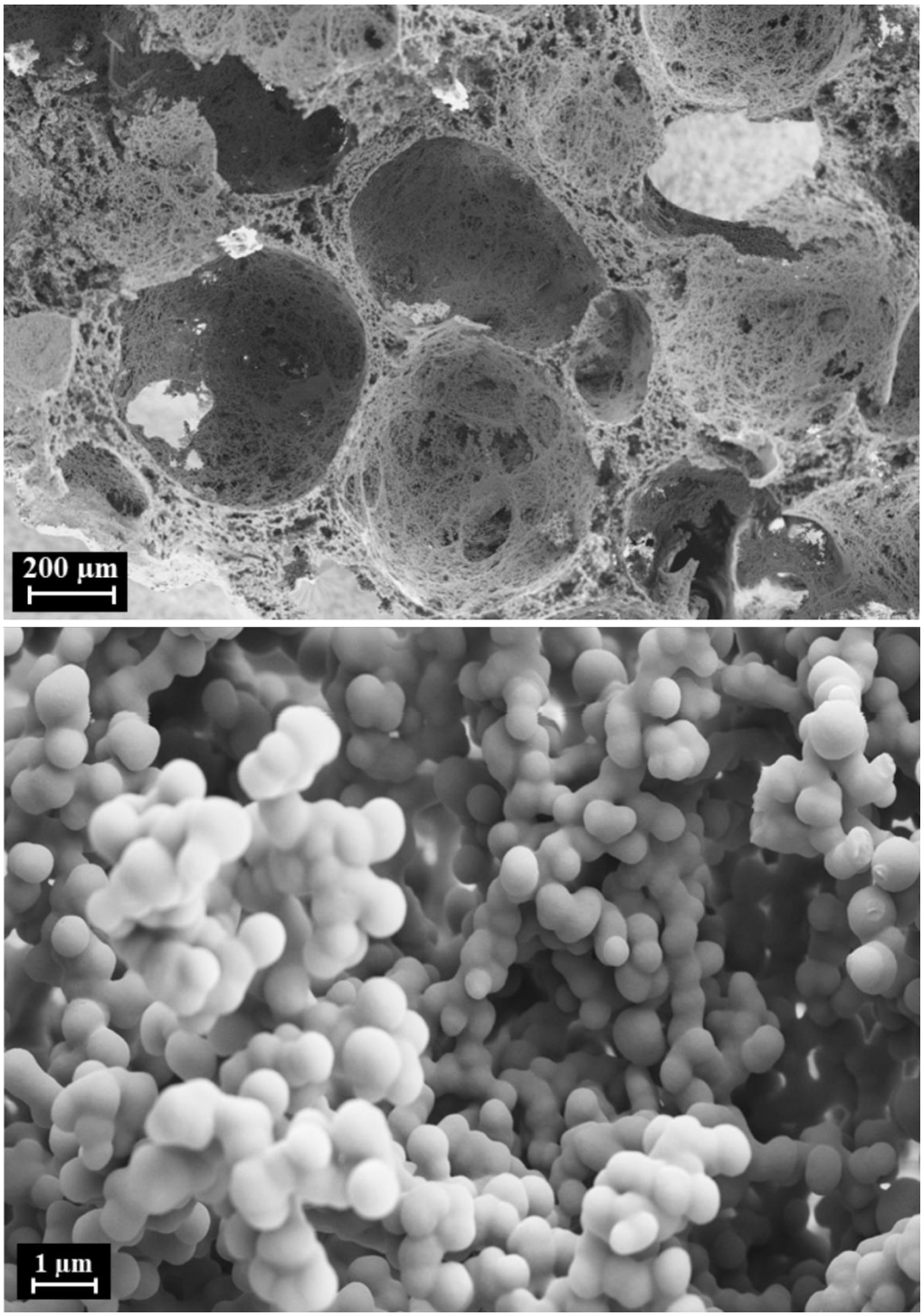

Figure S16. Morphology analysis of **4ea** foam by SEM.

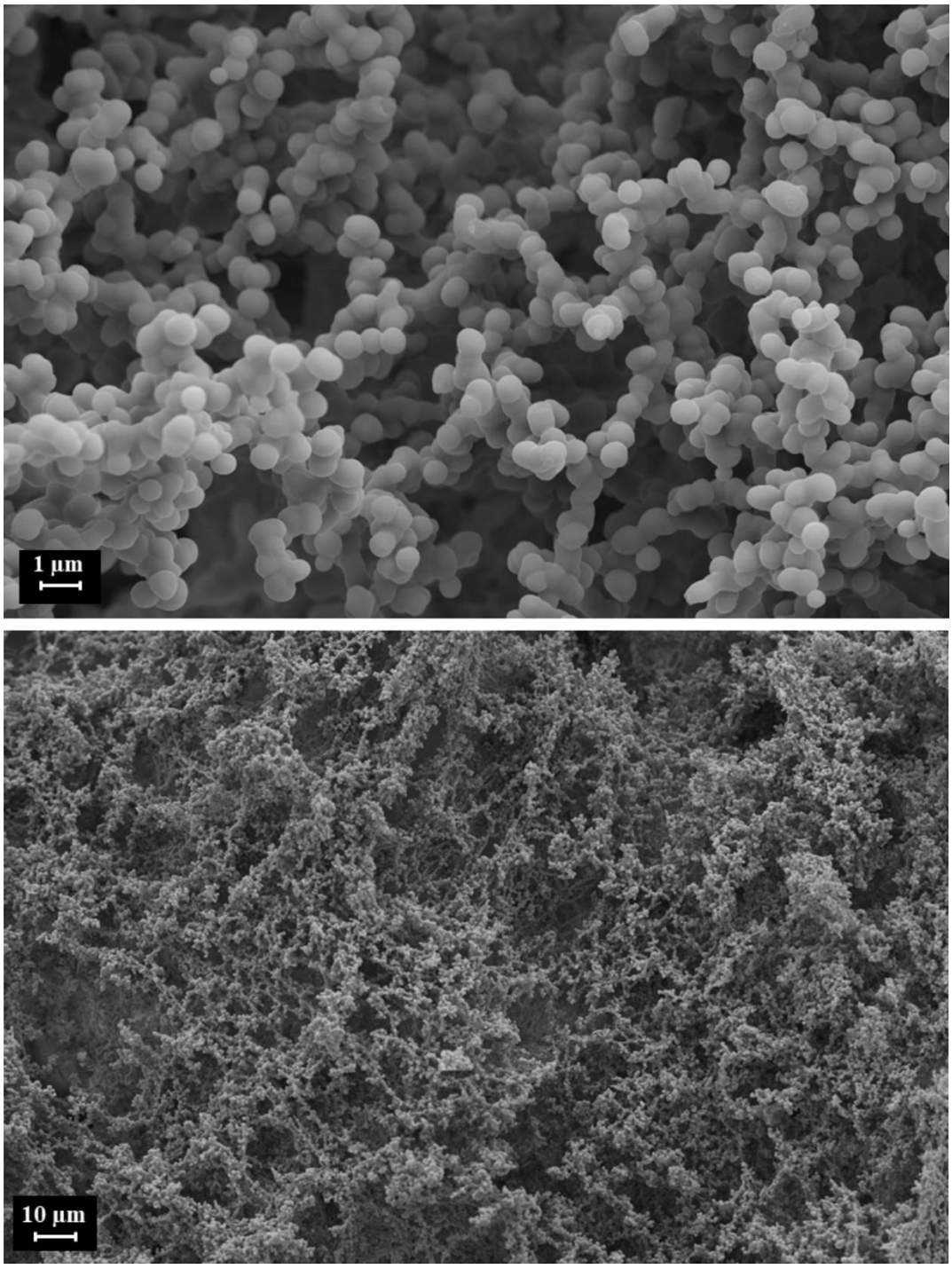

Figure S17. Morphology analysis of **4eb** foam by SEM.

XVII. Theoretical calculations

Theoretical calculations were performed using the density functional theory (DFT) and time-dependent DFT (TD-DFT), as implemented in Gaussian 16. For an accurate description of the organic and organo-metallic species, the wB97XD functional was used with a large 6-311+G(d,p) basis set, including polarization and diffusion functions. For detailed information on the electronic structure, especially orbital structure, NBO7 analyses were performed. For the calculation of the excited states, including optical band gaps and UV-Vis spectra, 30 excitations are taken into account and the first one is reported. The structures were geometrically optimised in the ground state and used in TD-DFT without further relaxation due to the computational cost required. Transition states were located with the STQN algorithm. Stable structures and transition state structures were optimised using vibrational analysis to contain exactly zero or one imaginary frequency, respectively. Larger (polymeric) structures were pre-optimized at the HF/6-31G level and fully re-optimized at the xB97XD/6-311+G(d,p) level. For the coordinates data see Supplementary data file.

Mechanism: energies

Table S2. Electronic energies of the intermediates. All values are in Hartree (as reported by Gaussian).

	AA	AB	BA	CA	EA	EB
Initial	-1431.785302	-2850.227958	-1938.198632	-1779.496417	-2124.751334	-3543.200774
Cis	-1431.787430	-2850.230753	-1938.206498	-1779.493490	-2124.744243	-3543.189341
Trans	-1431.782338	-2850.227947	-1938.195837	-1779.488166	-2124.739276	-3543.184918
Final	-1431.868732	-2850.313491	-1938.291891	-1779.576394	-2124.826432	-3543.271055
TS-cis	-1431.757679	-2850.202279	-1938.175653	-1779.463484	-2124.714320	-3543.158906
TS-trans	-1431.724172	-2850.167673	-1938.145853	-1779.433276	-2124.681764	-3543.125139
TS-iso	-1431.768638	-2850.213636	-1938.182362	-1779.474750	-2124.725357	-3543.170398
TS-one step	-1431.702572	-2850.150699	-1938.125856	-1779.408033	-2124.659421	-3543.107706
TS-final	-1431.754076	-2850.199925	-1938.171352	-1779.460562	-2124.711314	-3543.157344

Table S3. Gibbs free energies of the intermediates at 298.15 K and 1 atm. All values are in Hartree (as reported by Gaussian).

	AA	AB	BA	CA	EA	EB
Initial	-1431.461241	-2849.837588	-1937.888137	-1779.035817	-2124.198989	-3542.580491
Cis	-1431.458689	-2849.834586	-1937.889394	-1779.028992	-2124.190372	-3542.566580
Trans	-1431.455470	-2849.834768	-1937.882226	-1779.025566	-2124.187153	-3542.567147
Final	-1431.548277	-2849.926593	-1937.985461	-1779.119894	-2124.280669	-3542.658480
TS-cis	-1431.434360	-2849.812581	-1937.864517	-1779.004745	-2124.166070	-3542.541224
TS-trans	-1431.399937	-2849.775703	-1937.831794	-1778.970687	-2124.133031	-3542.508390
TS-iso	-1431.441233	-2849.820813	-1937.867758	-1779.011607	-2124.172787	-3542.551364
TS-one step	-1431.375212	-2849.756497	-1937.809826	-1778.944940	-2124.107124	-3542.487949
TS-final	-1431.425813	-2849.805403	-1937.855926	-1778.996697	-2124.158150	-3542.538371

XVIII. References

(59) Andjaba, J. M.; Rybak, C. J.; Wang, Z.; Ling, J.; Mei, J.; Uyeda. C. *J. Am. Chem. Soc.* **2021**, *143*, 3975–3982.

(60) Powers, I. G.; Andjaba, J. M.; Luo, X.; Mei, J.; Uyeda, C. *J. Am. Chem. Soc.* **2018**, *140*, 4110–4118.

(61) Bräse, S.; Gil, C.; Knepper, K.; Zimmermann, V. *Angew. Chem. Int. Ed.* **2005**, *44*, 5188–5240.

(62) Guo, X. Q.; Zhou, L. P.; Cai, L. X.; Sun, Q. F. *Chem. Eur. J.* **2018**, *24*, 6936–6940.

(63) Jordan, A.; Stoy, P.; Sneddon, H. F. *Chem. Rev.* **2021**, *121*, 1582–1622.

(64) Rothemund, S.; Teasdale, I. *Chem. Soc. Rev.* **2016**, *45*, 5200–5215.